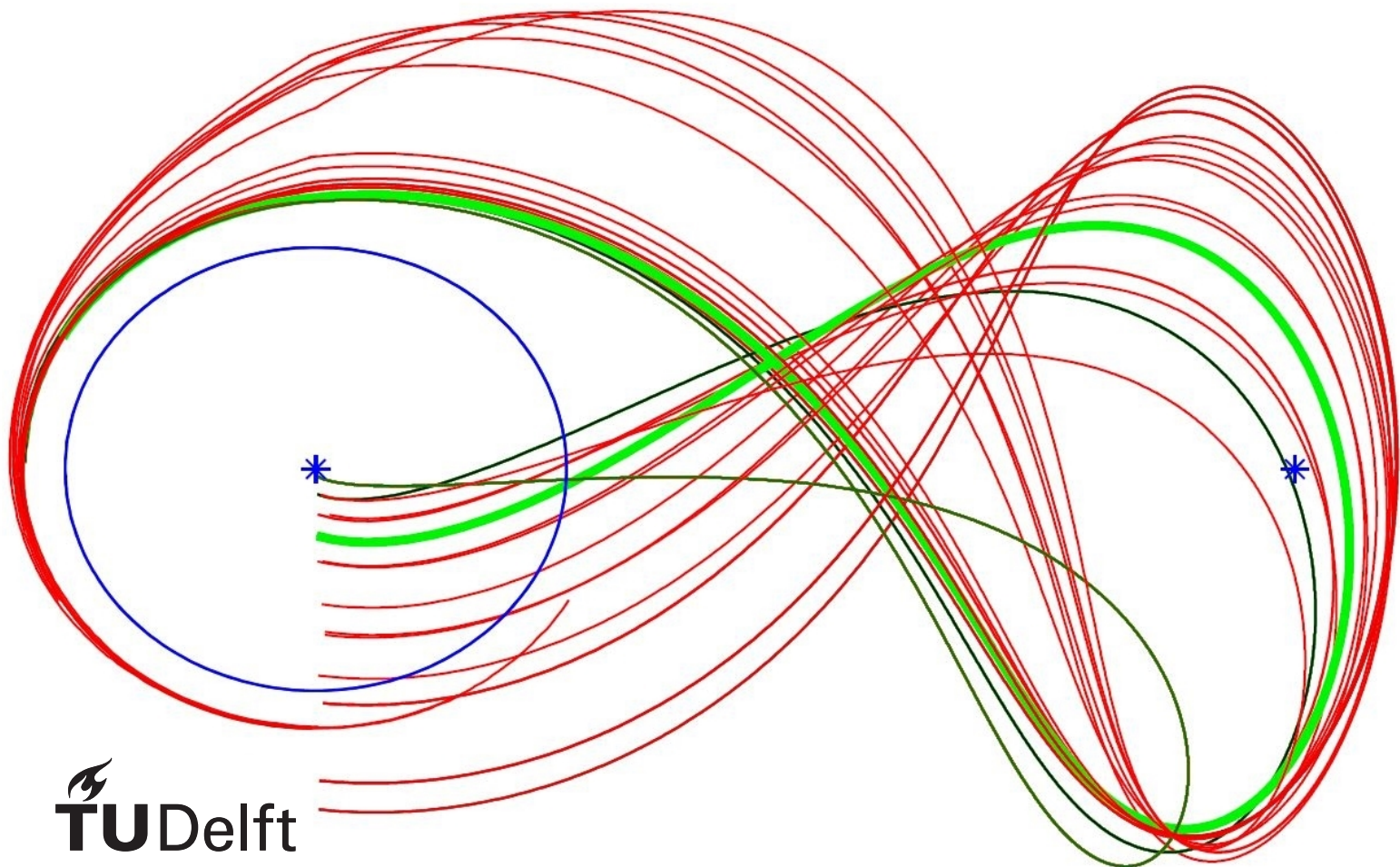


Combinations of Low Energy Trajectories for a Lunar L_2 mission

Thesis Report

A. M. Pronk



Combinations of Low Energy Trajectories for a Lunar L_2 mission

Thesis Report

by

A. M. Pronk

to obtain the degree of Master of Science
at the Delft University of Technology,
to be defended publicly on the 10th of Juli, 2018, at 10:00.

Student number: 4153243
Project duration: August, 2017 – Juli, 2018
Supervisor: dr. ir. B. C. Root, TU Delft

Preface

In recent years, the concept of small satellites has become more and more important to the industry of space-flight. But as we discover how to get more use out of ever smaller satellites, it also becomes more important to fly transfer trajectories that use minimal amounts of fuel. Traditional options such as Hohmann transfers are not viable for these missions, and so other options must be explored. Research into such options can deliver significant improvements in mission transfer trajectories, and provides an important base for future missions. It also allows the researcher to gain a deep understanding of the workings of a specific area of transfer design. This combination of factors has inspired me to look into this field of research, where I was introduced with the concept of low energy trajectories. Although the concept of such trajectories is not new, they have only been used a few times so far, and many possibilities have not yet been explored at all. With this knowledge, I set out into a search for improvements on the known uses of low energy trajectories.

During my entire thesis, I have encountered significant help. First and foremost I would like to thank my supervisor, Bart Root, for all the enthusiasm and continuously challenging me to go one step deeper into the research. Secondly, I would like to thank Dominic Dirkx for his help with the TU Delft Astrodynamics Toolbox. Thirdly, my thanks Ron Noomen for introducing me with the concept of low energy trajectories. And lastly, of course, all my friends who were there for me and provided me with motivation when I most needed it.

Abstract

To learn more about the origin of the universe, scientists wish to make measurements in the low-frequency radio wave region. Such measurements suffer greatly from disturbances by man-made signals. Therefore, missions are proposed which use the Moon as a shield from these disturbances, by making use of the Earth-Moon L_2 Lagrange point, a point in space behind the Moon in which spacecraft can remain stable with respect to the Earth and the Moon. Especially missions using large numbers of small satellites are considered valuable, because such groups could together work as an antenna with a very large aperture, which is beneficial for low-frequency measurements.

This research explores the use of low energy trajectories for a mission to the Earth-Moon L_2 point. Low energy trajectories are found in the circular restricted three body problem, originating in the vicinity of the Lagrange points. They may be divided into four classes: The periodic ellipse around the Lagrange point, asymptotic trajectories spiralling into or out of this ellipse, non-transit trajectories which stay either on the main body's side of the Lagrange point or stay on the other side, and the transit trajectories which move from one side of the Lagrange point to the other.

Although low energy trajectories have been researched for 50 years and used in missions such as Hiten and Genesis, there has hardly been research on the use of low energy trajectories for a mission to the Earth-Moon L_2 point. This leads to the following research question: *What is the optimal configuration for a low energy transfer for a small satellite mission from an Earth-orbit to a lunar L_2 orbit, when allowing for ballistic and non-ballistic transfers?* The research assumes that the launcher vehicle will inject the small satellite into the transfer trajectory.

The design of the mission transfer trajectory using low energy trajectories can be performed with different approaches. Each approach uses a combination of the low energy trajectory categories. Four configurations are considered:

1. The standard approach found in literature, which uses a non-transit trajectory in the Sun-Earth system coupled at the vertical Poincaré cut through the Earth with an asymptotic trajectory approaching the Earth-Moon L_2 in the Earth-Moon system.
2. An approach with three asymptotic trajectories, which first travels to the Sun-Earth L_2 point, then back in the direction of Earth, to be coupled to a final segment in the Earth-Moon system to arrive at the Earth-Moon L_2 point.
3. An approach that uses the same segments as the standard approach, but that allows the location of the link between segments to be at any point instead of only on the vertical Poincaré cut.
4. An approach which allows up to six linked trajectories and has no restriction on the classes of low energy trajectories used or the location of their links.

These four low energy transfer configurations were compared to answer the research question. The first comparison is made based on ΔV . Here we see that the third approach is most efficient with a ΔV below 10 m/s (standard approach: 30 m/s). The second comparison, on transfer time, also shows that the third approach is the most efficient, with a total transfer time of approximately 120 days (standard approach: 140 days). Third, we look at the scheduling restrictions: How much does ΔV increase when the moment of launch changes. Clearly optimal here is the second approach, which allows for a station-keeping orbit around the Sun-Earth L_2 point. Lastly, we look at the location of orbit insertion. Insertion near to the Earth means that the launcher requires less ΔV , which is beneficial for total mission cost. Again, the third approach performs best, with a starting point at a distance of 11,790 km from the Earth.

It can then be concluded that the third approach is the optimal configuration for a low energy transfer for a small satellite mission from an Earth-orbit to a lunar L_2 orbit. However, when additional mission objectives can be performed at the Sun-Earth L_2 , the second approach might be a good alternative. In general, this research has shown that significant improvements over the standard approach found in literature are possible.

Contents

Preface	iii
Abstract	v
Nomenclature	x
1 Introduction	1
2 Underlying Physics: The CR3BP	5
2.1 Three Body Problems	5
2.2 The Circular Restricted Three Body Problem	5
2.3 Lagrange Libration Points	10
3 Creating Low Energy Trajectories: Dynamical Systems Theory	15
3.1 Linearisation of the CR3BP	15
3.2 Transformation of CR3BP to Subspaces	17
3.3 Classes of Trajectories in the Subspaces	18
3.4 Classes of Trajectories in the CR3BP	19
3.5 Implementation of trajectories in TUDAT	20
4 Creating Low Energy Transfers: Trajectory Linking	23
4.1 Standard approach	23
4.2 Three asymptotic segments	24
4.3 Free location of linking	25
4.4 All classes, all link locations	26
5 Complete Low Energy Transfers: Results	29
5.1 Standard approach	29
5.2 Three asymptotic segments	32
5.3 Free location of linking	34
5.4 All classes, all link locations	37
5.5 Robustness	40
6 Comparing Low Energy Transfers: Discussion	43
6.1 Comparison of ΔV and transfer time	43
6.2 Comparison of scheduling	44
6.3 Comparison of transfer starting point	45
6.4 Complete comparison	46
7 Conclusions and Recommendations	49
7.1 Conclusions of the research	49
7.2 Reflection on the methods	49
7.3 Recommendations for future work	50
A Appendix: Trajectory creation script details	51
A.1 Constants	51
A.2 Ephemeris Creation	51
A.3 Initial Conditions Calculation	52
A.4 Propagation	54
Bibliography	54

Nomenclature

Acronyms

3BP	Three Body Problem
CR3BP	Circular Restricted Three Body Problem
IPS	Interplanetary Superhighway System
L_1	First Lagrange Point
L_2	Second Lagrange Point
L_3	Third Lagrange Point
L_4	Fourth Lagrange Point
L_5	Fifth Lagrange Point
ODE	Ordinary Differential Equation
OLFAR	Orbiting Low-Frequency Antennas for Radio astronomy
R3BP	Restricted Three Body Problem
TUDAT	TU Delft Astrodynamics Toolbox

Greek Symbols

α	constant used for simplification	[-]
α_1	real constant	[-]
α_2	real constant	[-]
β	constant used for simplification	[-]
β	complex constant	[-]
γ_1	factor used for finding L_1 (see Figure 2.4)	[-]
γ_2	factor used for finding L_2 (see Figure 2.4)	[-]
γ_3	factor used for finding L_3 (see Figure 2.4)	[-]
Δ	change of the following variable	[-]
δ	infinitesimal change of the following variable	[-]
ζ_1	coordinate on the w_1 axis	[-]
ζ_2	coordinate on the w_2 axis	[-]
η	coordinate on the u_2 axis	[-]
κ	real constant	[-]
λ	eigenvalue	[-]
μ	unit of mass	[-]
μ	gravitational parameter	m^3s^{-2}
ν	frequency	Hz
ν	positive constant	[-]
ξ	coordinate on the u_1 axis	[-]
ω	angular velocity	$rad\ s^{-1}$
ρ	constant used for simplification	[-]
σ	constant	[-]
τ	constant	[-]

Latin Symbols

a	constant used for simplification	[-]
b	constant used for simplification	[-]
C	complex number	[-]
C	Jacobi's constant	[-]
E	Energy integral of the Hamiltonian	J
e_x	unit vector in x-direction	[-]
e_y	unit vector in y-direction	[-]
e_z	unit vector in z-direction	[-]
G	gravitational constant	$m^3 kg^{-1} s^{-2}$
H	Hamiltonian function	J
i	$\sqrt{-1}$	[-]
k	x-coordinate of Lagrange point	[-]
m	mass	kg
O	barycentre location	[-]
P_1	Heaviest body in a 3BP	[-]
P_2	Second heaviest body in a 3BP	[-]
P_3	Least heavy body in a 3BP	[-]
p_x	momentum variable	N
p_y	momentum variable	N
\mathbb{R}	real number	[-]
r	distance between two bodies	m or [-]
r	orbital radius	m
S	set	[-]
t	time	sec
T_c	orbital period for circular orbits	sec
U	scalar function of spatial coordinates	[-]
u_1	axis of the manifold subspace	[-]
u_2	axis of the manifold subspace	[-]
V	velocity	$m s^{-1}$
w_1	axis of the manifold subspace	[-]
w_2	axis of the manifold subspace	[-]
x	location coordinate on the x-axis	m
\dot{x}	velocity in the direction of the x-axis	ms^{-1}
\ddot{x}	acceleration in the direction of the x-axis	ms^{-2}
y	location coordinate on the y-axis	m
\dot{y}	velocity in the direction of the y-axis	ms^{-1}
\ddot{y}	acceleration in the direction of the y-axis	ms^{-2}
z	location coordinate	m or [-]
\dot{z}	velocity in the direction of the z-axis	ms^{-1}
\ddot{z}	acceleration in the direction of the z-axis	ms^{-2}

1

Introduction

Scientists are intrigued by the origin of our universe. To obtain more information about, low-frequency radio waves, below 30 MHz, are measured. In this region, not only the 'dark ages' (early cosmos) can be measured at high hydrogen red-shifts, but a view of space-weather, solar bursts in other solar systems and new exo-planets may be found (Bentum et al., 2009). Unfortunately measurements in this frequency band have proven difficult to obtain, since the ionosphere scatters and reflects these signals, and because human-made signals interfere with the signals from space. Measurements from the Earth itself are useless for these studies. The ionospheric disturbance in an Earth orbit is also too great (Jester and Falcke, 2009) (Alexander et al., 1975).

The difficulty of measuring low-frequency radio waves from Earth orbits, is one of the reasons why scientists are proposing missions to an orbit 'behind' the Moon, where satellites are shielded from terrestrial interference (Engelen et al., 2010). Missions such as the Orbiting Low-Frequency Antennas for Radio astronomy (OLFAR) propose satellite trajectories around the second Earth-Moon Lagrange point (L_2) (Vermeiden, 2014) (Bentum et al., 2009). Satellites in such trajectories are shielded from terrestrial interference most of the time, but at the tips of their elliptic trajectories they have a direct line of sight with the Earth to allow direct communications.

An additional challenge for measuring low-frequency radio waves is the required aperture of the antenna, which is in the range of kilometres (Dekens et al., 2014). This is not possible to reach with a single satellite. However, a swarm of small satellites flying in specific formations may result in a similar quality of data. Although Jester and Falcke (2009) predicts that an order of $10^4 - 10^8$ antennas would be required for ideal results, a lot of science could already be performed with a thousand satellites, which is a far less improbable number (Engelen et al., 2010).

The challenge for such missions is to get large numbers of small satellites into an orbit around the Earth-Moon L_2 Lagrange point. The traditional high thrust method of transfer for a mission to the Earth-Moon L_2 Lagrange point would be a Hohmann transfer (Szebehely and Mark, 1998). The first burn of the Hohmann can be performed by the launcher. The second burn, which slows down the satellite into the desired trajectory, must be performed by the satellite itself, and requires a ΔV of about 1 km/s (Riesbroek and Janin, 2000). Most small satellites are not capable of delivering this amount of ΔV due to limited fuel storage and engine size. The traditional low thrust method of transfer would be a slowly widening spiral around Earth (Betts and Erb, 2003). Such transfers are very complex when encountering three body dynamics (Ozimek and Howell, 2010). It is thus required to look at non-traditional options. The 1991 Hiten mission proved that it is also possible to use a transfer made up of so-called 'low energy trajectories', which make use of the perturbation of a third body (Uesugi et al., 1991).

Conley (1968) was amongst the first to describe the concept of low energy trajectories in the restricted three body problem. It was further developed by, amongst others, Lo and Ross (2001), who describe this type of trajectories as the "Interplanetary Superhighway System" (IPS). These low energy trajectories form 'tunnels' throughout the solar system, running around the Sun, planets and Moon, originating

in the vicinity of the Lagrange Points. Belbruno (2004) describes how manifold trajectories may be used in space mission, including applications for escape and capture trajectories.

Low energy trajectories are found on the invariant manifolds of the circular restricted three body problem (CR3BP). An invariant manifold is a subspace of the solution space of a problem (Wiggins, 2003) (Abraham et al., 1990). This subspace has two main characteristics: First of all, it has less dimensions than the solution space. Second, any solution that is at any point in this subspace, is in the subspace for all points. Thus, an invariant manifold of the CR3BP is a collection of trajectories which can be found in a subspace of the CR3BP. Trajectories that are in this subspace at any point do not leave it without forces acting on it. Thus, if a solution to the equations of motion in the subspace can be found, a set of trajectories are found through the CR3BP for which no burns are needed.

Koon et al. (2001) proved that using low energy transfers over invariant manifolds could decrease the required fuel by around 20% when comparing to the Hohmann transfer, with the majority of required fuel used up when injecting into the trajectory from an Earth orbit and no burn needed at the end of the trajectory to insert into the orbit around the Earth-Moon L_2 . This is especially beneficial for small satellites, for which the launcher vehicle could provide the initial boost away from Earth.

The use of low energy trajectories over invariant manifolds for a transfer to the L_2 point of the Moon has been demonstrated by several mission. Most famous amongst them are Genesis (Lo and Ross, 2001) and Hiten (Koon et al., 2001). Research has also been done into the design and optimisation of such transfers, amongst others by Parker (2007), Mingotti et al. (2011) and Davis et al. (2013). Both the missions and the research uses transfer trajectories of two different low energy trajectory segments. The first segment starts near the Earth, then passes close to the Sun-Earth L_2 Lagrange point before going back into the direction of Earth. At a specified location, the spacecraft transfers to a trajectory towards the Earth-Moon L_2 point. In theory, this transfer can be performed without the need of a burn. Therefore, such transfer trajectories are named 'ballistic low energy transfers'. In reality, a small burn in the order of 20-40 m/s is required to perform the transfer (Koon et al., 2001). Nonetheless, such transfers are still considered 'ballistic'. A few examples of such transfers are shown in Figure 1.1.

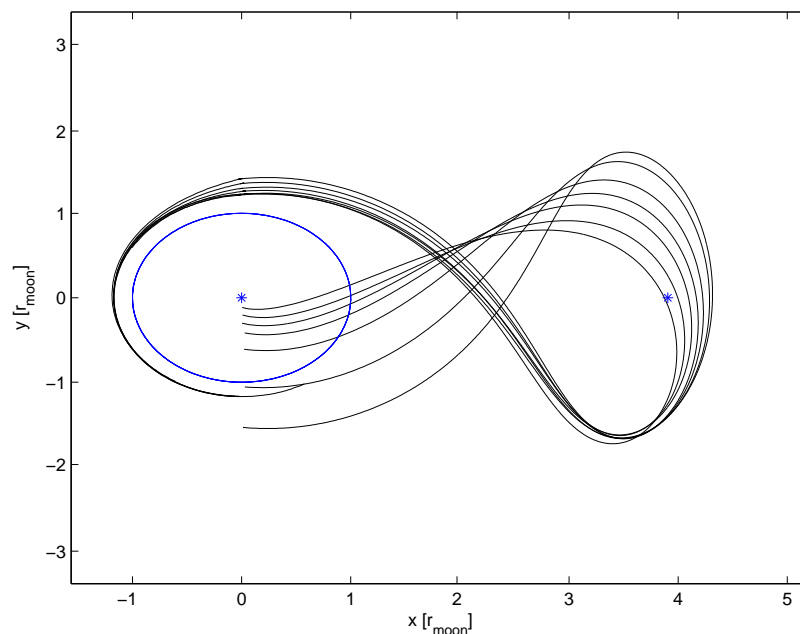


Figure 1.1: Examples of low energy ballistic transfers from the Earth to an Earth-Moon L_2 orbit. The blue asterisk at the origin is the Earth, the blue circle around this is the orbit of the Moon. The blue asterisk on the positive x-axis is the Sun-Earth L_2 Lagrange point. The Sun is positioned on the negative x-axis. All other, black lines in the figure are low energy ballistic transfers. Transfers start on the negative y-axis and end at the Earth-Moon L_2 Lagrange point.

The researched low energy trajectories have always been of the ballistic type. However, there are several types of possible transfer layouts using low energy trajectories which are not ballistic. Such layouts could make it possible for the satellite to enter an ellipse around the Sun-Earth Lagrange point for some time, either for scheduling purposes or for additional research. (Parker, 2007) suggest that it might be possible to reduce the amount of change in velocity (ΔV) required by replacing the single transition of the ballistic transfer with several transitions requiring even smaller burns, and urges for additional research in this area. For this research, such transfers with more than one transition are named 'non-ballistic low energy transfers'. Non-ballistic options have never been researched in published work, and are one of the two focusses of this research.

The traditional ballistic low energy transfer uses a specified location for the link between the two segments of the transfer. There has been some research into the advantages of changing the location of this link, for missions towards the Sun-Earth L_1 and/or L_2 . For such missions it has been shown that a decrease in required ΔV is possible when changing the link location (Langemeijer, 2018). Such research has not yet been performed for the transfer to the Moon. Such work is the second focus of this research.

This report on possible alterations on the 'standard' low energy transfer from the Earth to the Earth-Moon L_2 , with the aim of finding feasible transfers for low frequency measurement missions. The main research question is thus formulated as follows:

What is the optimal configuration for a low energy transfer for a small satellite mission from an Earth-orbit to a lunar L_2 orbit, when allowing for ballistic and non-ballistic transfers?

Note that this means the research is not meant to find the optimal transfer itself: The research is limited to looking at different configurations and comparing them, after which a conclusion may be reached on the optimal configuration. This research question is answered using four sub-questions, each concerning a possible configuration for the transfer:

1. What is the range for ΔV and transfer time, for the 'standard' ballistic transfer?
2. What is the range for ΔV and transfer time, for the ballistic transfer, when the location of the transfer from the first section to the second section is allowed to vary?
3. What is the range for ΔV and transfer time, for a non-ballistic transfer with three segments (Earth - Sun-Earth L_2 , Sun-Earth L_2 - Moon influence, Moon influence - Earth-Moon L_2)?
4. What is the range for ΔV and transfer time, for a non-ballistic transfer with up to five burns in unspecified locations?

The first sub-question is used for validation of the results, since there has been some previous research into transfers with such lay-outs. The subsequent sub-questions each present a new, not yet researched configuration for the transfer.

It should be noted that each of the questions is about the required ΔV and transfer time for the transfer, only. This means that the injection into this transfer is not taken into account. This is done because it is likely that the injection into the transfer is performed by the launcher vehicle instead of the satellite itself. This research seeks to minimize the ΔV for the satellite, because many of the missions that will use transfers such as these will involve small satellites with very limited fuel resources.

Several assumptions will be made to allow for answering the research question. Most important of these is that the trajectories of the Sun, Earth and Moon are assumed to be planar and circular, and that each of these bodies are treated as point masses. The second important assumption is that the transition between two three body problems is instant: At one moment the spacecraft is influenced by the Sun and the Earth, and at the next moment it is influenced by the Earth and the Moon. These two assumptions greatly simplify the mathematics and allows the entire research to take place in a two dimensional environment. It should be noticed that it also limits the options for the types of low energy trajectories used. However, for the comparison between transfer layouts, the two dimensional environment is sufficient. It should also be noticed that the simplifications used result in transfers that

are not directly of use in real life missions. However, the purpose of this report is that of comparison of methods, not of transfer design.

The report starts with explaining the theory of low energy trajectories. The basic physics of the CR3BP and Lagrange points are explained in Chapter 2, followed by the dynamical systems theory used to create low energy trajectories in Chapter 3. Both chapters also include the implementation of these concepts into a model. Making use of the trajectories created through these chapters, it is possible to start combining trajectories into complete transfers. The different approaches to trajectory linking are explained in Chapter 4, and the results of these approaches are discussed in Chapter 5. This Chapter also discusses the validation of the trajectories and transfers, and a discussion on the robustness of the model. Chapter 6 then describes the comparison between the results of different approaches, and the implications to the research question. This leads to a conclusion to the research in Chapter 7.

2

Underlying Physics: The CR3BP

The theory of low energy trajectories builds on the Circular Restricted Three Body Problem (CR3BP) and its equilibria. This problem describes a small body following a trajectory about two larger bodies which both follow a circular orbit around the barycentre of the system. Within the CR3BP, the Lagrange Libration points are found. Low energy trajectories originate from the Lagrange points. As such, an understanding of these points and the underlying CR3BP is fundamental to understanding how the low energy trajectories are found.

2.1. Three Body Problems

The three body problem describes the motion of three bodies in space. It was first described in the Principia by Newton (1687). After this, many people have tried solving the problem with no success, until it was proven by Bruns (1887) that there could be no algebraic function to describe the problem, and by Poincaré (1893) that there could be no analytical solution to the problem either. This led to the simplifications of the problem described in Section 2.2.

The general Three Body Problem describes how three given point masses move under their mutual gravitational attraction. The three bodies are named P_1 , P_2 and P_3 , and have masses m_1 , m_2 and m_3 . When placed into the standard inertial XYZ frame with the origin in the centre of mass, and using Newtons laws, this gives the following equation for the motion of each of the bodies (Wakker, 2015, page 45-49):

$$\frac{d^2 \vec{r}_i}{dt^2} = G \frac{m_j}{r_{ij}^3} \vec{r}_{ij} + G \frac{m_k}{r_{ik}^3} \vec{r}_{ik} \quad (2.1)$$

Where t is time, \vec{r}_i is the distance of body P_i to the origin, \vec{r}_{ij} the distance between bodies P_i and P_j , and G is the universal gravitational constant.

Although the three body problem can be solved numerically, it can only be solved algebraically or analytically for some special cases, such as the case wherein the bodies are on an equilateral triangle (Lagrange case), and the case wherein the three bodies are on a straight line (Euler case). More general information about the three body problem can for example be found in Poincaré (1893) or Wakker (2015).

2.2. The Circular Restricted Three Body Problem

The CR3BP is one of the possible simplifications on the three body problem (Wakker, 2015, page 55-59). It is described briefly in Section 2.2.1, in order to understand further information concerning the manifold orbits. Then, the implementation of the CR3BP into the code used for the research is explained in Section 2.2.2.

2.2.1. Equations of motion of the CR3BP

In the CR3BP, three bodies are present, which we shall call P_1 , P_2 and P_3 . It is assumed the masses of the first two bodies, m_1 and m_2 , are so much larger than the mass of the third body, m_3 , that the gravitational effects of m_3 on the system can be neglected. Also, it is assumed that the larger bodies are in circular orbits around the barycentre of the system. Since the mass of the third body is neglected, the two remaining masses represent a simple two body problem. Using the solutions for the two body problem described by Wakker (2015), we can determine that both bodies rotate around the barycentre at the same, constant angular velocity.

The CR3BP uses a reference frame with the origin at the barycentre, which rotates at the same angular velocity as the two main bodies. The X-axis is the line between P_1 , the barycentre, and P_2 , with the positive direction from the barycentre towards P_2 . The Z-axis is the axis around which the system rotates. In this system, P_1 and P_2 always remain on the same location on the X-axis. P_3 is free to move in each of the three dimensions. This system is shown in Figure 2.1.

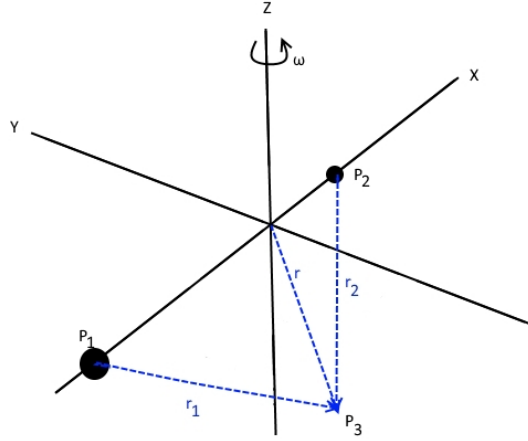


Figure 2.1: Coordinate system of the CR3BP. P_1 and P_2 are the main bodies, which are placed on the x-axis. The entire system rotates at a rate ω around the z-axis. P_3 is the spacecraft which moves freely.

In this system, distances r , r_1 and r_2 are also defined. They are the distances from P_3 to, respectively, the origin, P_1 and P_2 . With this knowledge, the equation of motion of the body P_3 with respect to the rotating reference frame can be determined:

$$\frac{\delta^2 \vec{r}}{\delta t^2} = -G \left(\frac{m_1}{r_1^3} \vec{r}_1 + \frac{m_2}{r_2^3} \vec{r}_2 \right) - 2\vec{\omega} \times \frac{\delta \vec{r}}{\delta t} - \vec{\omega} \times (\vec{\omega} \times \vec{r}) \quad (2.2)$$

Where ω is the angular velocity of the two bodies in the inertial reference system. The first term on the right hand side is the motion of the body had it been in a inertial reference frame. The second term is the Coriolis acceleration. The third term is the centrifugal acceleration. These last terms are introduced due to the rotation of the system. Because the system rotates at a constant rate, there is no Euler acceleration.

The system is simplified by the use of different units of mass. We set $(m_1 + m_2)$ as a unit of mass, and introduce the unitless variable μ to get:

$$m_1 = 1 - \mu \quad (2.3)$$

$$m_2 = \mu \quad (2.4)$$

As a unit of length, we use the distance between P_1 and P_2 . Then, since O is the barycentre, the following holds:

$$\frac{OP_1}{OP_2} = \frac{m_2}{m_1} = \frac{\mu}{1 - \mu} \quad (2.5)$$

$$OP_1 = \mu \quad (2.6)$$

$$OP_2 = 1 - \mu \quad (2.7)$$

Lastly, we set a unit of time as $1/\omega$. Then, we rewrite equation 2.2, using the new units for r and t , to get:

$$\frac{\delta^2 \bar{r}}{\delta t^2} = -\frac{G}{\omega^2} \left[\frac{1-\mu}{r_1^3} \bar{r}_1 + \frac{\mu}{r_2^3} \bar{r}_2 \right] - 2\bar{e}_z \times \frac{\delta \bar{r}}{\delta t} - \bar{e}_z \times (\bar{e}_z \times \bar{r}) \quad (2.8)$$

Here \bar{e}_z is the unit vector in the direction of the z-axis.

This can be further simplified when we use the equation for the circular motion of body P2:

$$m_2 \omega^2 (OP_2) = G \frac{m_1 m_2}{(P_1 P_2)^2} \quad (2.9)$$

Which we can translate to:

$$\frac{G}{\omega^2} = \frac{(OP_2)(P_1 P_2)^2}{m_1} = \frac{1-\mu}{1-\mu} = 1 \quad (2.10)$$

Combining equations 2.8 and 2.10 gives:

$$\frac{\delta^2 \bar{r}}{\delta t^2} = \left[\frac{1-\mu}{r_1^3} \bar{r}_1 + \frac{\mu}{r_2^3} \bar{r}_2 \right] - 2\bar{e}_z \times \frac{\delta \bar{r}}{\delta t} - \bar{e}_z \times (\bar{e}_z \times \bar{r}) \quad (2.11)$$

From the coordinate system that was defined, we know:

$$\bar{r}_1 = (\mu + x)\bar{e}_x + y\bar{e}_y + z\bar{e}_z \quad (2.12)$$

$$\bar{r}_2 = -(1 - \mu - x)\bar{e}_x + y\bar{e}_y + z\bar{e}_z \quad (2.13)$$

$$\bar{r} = x\bar{e}_x + y\bar{e}_y + z\bar{e}_z \quad (2.14)$$

$$\frac{\delta \bar{r}}{\delta t} = \dot{x}\bar{e}_x + \dot{y}\bar{e}_y + \dot{z}\bar{e}_z \quad (2.15)$$

$$\bar{e}_z \times \frac{\delta \bar{r}}{\delta t} = \dot{x}\bar{e}_y - \dot{y}\bar{e}_x \quad (2.16)$$

$$\bar{e}_z \times (\bar{e}_z \times \bar{r}) = -x\bar{e}_x - y\bar{e}_y \quad (2.17)$$

Here, x , y and z are the locations of the spacecraft on each axis, \bar{e}_x is the unit vector in the direction of the x-axis, \bar{e}_y is the unit vector in the direction of the y-axis and dots are used to indicate derivatives to time.

Equations 2.12 through 2.17 can be used to rewrite equation 2.11 into three scalar equations:

$$\ddot{x} - 2\dot{y} = x - \frac{1-\mu}{r_1^3}(\mu + x) + \frac{\mu}{r_2^3}(1 - \mu - x) \quad (2.18)$$

$$\ddot{y} + 2\dot{x} = y - \frac{1-\mu}{r_1^3}y - \frac{\mu}{r_2^3}y \quad (2.19)$$

$$\ddot{z} = -\frac{1-\mu}{r_1^3}z - \frac{\mu}{r_2^3}z \quad (2.20)$$

Where double dots are used to indicate second derivatives to time. Then the scalar function U is introduced (Koon et al., 1999):

$$U = \frac{1}{2}(x^2 + y^2) + \frac{1-\mu}{r_1} + \frac{\mu}{r_2} + \frac{\mu(1-\mu)}{2} \quad (2.21)$$

Wakker (2015) formulates this function slightly different (equation 2.22), in a manner that is sufficient for the problem at hand in his work. However, equation 2.21 is more complete. In following steps, this more complete notation allows for additional simplifications, such as in equations 2.29 and 2.30. The shorter version of Wakker does not result in these simple equations.

$$U_{Wakker} = \frac{1}{2}(x^2 + y^2) + \frac{1-\mu}{r_1} + \frac{\mu}{r_2} \quad (2.22)$$

By using partial differentiation of equation 2.21 and comparing to equations 2.18 through 2.20 we get:

$$\ddot{x} - 2\dot{y} = \frac{\partial U}{\partial x} \quad (2.23)$$

$$\ddot{y} + 2\dot{x} = \frac{\partial U}{\partial y} \quad (2.24)$$

$$\ddot{z} = \frac{\partial U}{\partial z} \quad (2.25)$$

Equations 2.21, 2.23, 2.24 and 2.25 together describe the solution to the CR3BP.

Chapter 3 will show that the system of equations must be linearised to find low energy trajectories. In preparation of this, the system above may be written in a simplified form, which is easier to linearise. For this purpose the Hamiltonian function, a measure of the energy of the system, is mentioned here. The Hamiltonian of the system described above is found to be (Koon et al., 2000b):

$$H = \frac{(p_x + y)^2 + (p_y - x)^2}{2} - \frac{x^2 + y^2}{2} - \frac{1-\mu}{r_1} - \frac{\mu}{r_2} - \frac{\mu(1-\mu)}{2} \quad (2.26)$$

Here, variables p_x and p_y are introduced. They are created to simplify the equation and are defined with respect to location and velocity as follows:

$$\dot{x} = \frac{\delta H}{\delta p_x} = p_x + y \quad (2.27)$$

$$\dot{y} = \frac{\delta H}{\delta p_y} = p_y - x \quad (2.28)$$

$$\dot{p}_x = -\frac{\delta H}{\delta x} = p_y - x + \frac{\partial U}{\partial x} \quad (2.29)$$

$$\dot{p}_y = -\frac{\delta H}{\delta y} = -p_x - y + \frac{\partial U}{\partial y} \quad (2.30)$$

This set of equations describes exactly the same system as equations 2.23 through 2.25, but in a form that allows for very easy linearisation, as will be shown in Chapter 3.

2.2.2. Implementation of the CR3BP in TUDAT

The low energy trajectories will be calculated through propagation from a starting position, as will be explained in Chapter 3. For this purpose, an ephemeris model must be created that fits to the CR3BP. This is done using the TU Delft Astrodynamics Toolbox (TUDAT (Delft University of Technology, 2016)), which provides a functional base for such work and allows for re-use of the written code for later re-search at the TU Delft or associated parties.

The ephemeris model that was created is not a direct implementation of the CR3BP. TUDAT works with an inertial reference frame, not with the rotating frame of the CR3BP. Therefore, the ephemeris model uses rotating circular orbits for the main bodies. While this does not influence the forces on and motion of a spacecraft with respect to the bodies, the coordinates changes. This has to be taken into account when the initial conditions are calculated.

$$T_c = 2\pi \sqrt{\frac{r^3}{\mu}} \quad (2.31)$$

For this research, two ephemeris models are created: One with the Sun and the Earth as the main bodies, and one with the Earth and the Moon as the main bodies. The bodies are created with the gravitational parameters (μ) and orbital periods (T_c) as defined by TUDAT, which can be found in Table 2.1. From these constants, and being restricted to circular orbits, the radius of the orbits (r) can be calculated using equation 2.31 (Wakker, 2015). This creates the constants for the three main bodies found in Table 2.1.

Table 2.1: Ephemeris model constants for the three main bodies

	$\mu [m^3s^{-2}]$	T_c [sec]	r [m]
Sun	$1.3271244 \cdot 10^{20}$		
Earth	$3.9860044 \cdot 10^{14}$	31558149.5	149597873474.7
Moon	$4.9048695 \cdot 10^{12}$	2354175.3	384051120.5

In each of the models, the larger of the two bodies is located at the origin of the coordinate system. The other body is given a constant circular orbit around the origin, using the orbital period and radius as described above. At $t = 0$ the secondary body is placed on the positive x-axis, then moves counter-clockwise over the xy-plane. Any third body placed within this system will feel the attraction of each of the two larger bodies, but it will not affect the orbits of the two main bodies, as befits the third body in the CR3BP. For more details on the written script, refer to Appendix A.2.

To verify both the models, it was checked if the trajectories are truly circular, by plotting the change in distance between the two bodies. These plots are shown in Figures 2.2a and 2.2b for the Sun-Earth and Earth-Moon system respectively. These plots show erratic behaviour, caused by the rounding errors of the numerical approximation of circular trajectories. There is no drift visible on the long term, nor are there strange outliers. Figure 2.2b shows some periodic behaviour, with a period equal to half the orbit period of the Moon. The error is larger when the Moon is in line with Earth and the Sun. This is caused by the way the data are saved in the script: The location of the Moon is first saved relative to the Sun, then is converted to be relative to the Earth. Because the Earth and the Moon both start on the positive x-axis, the x coordinate of the Moon is far larger than the y coordinate at the start of the run. Due to the way TUDAT saves coordinates, this results in larger rounding errors. If the plot were to extend to more orbital periods, it would become visible that the peaks changed to the positions where the Moon is on the y-axis relative to the Earth, due to it's location with respect to the Sun changing. We can thus conclude that the erratic behaviour is indeed due to rounding errors and will not show drift. Therefore, the trajectories are considered sufficiently precise on the long term.

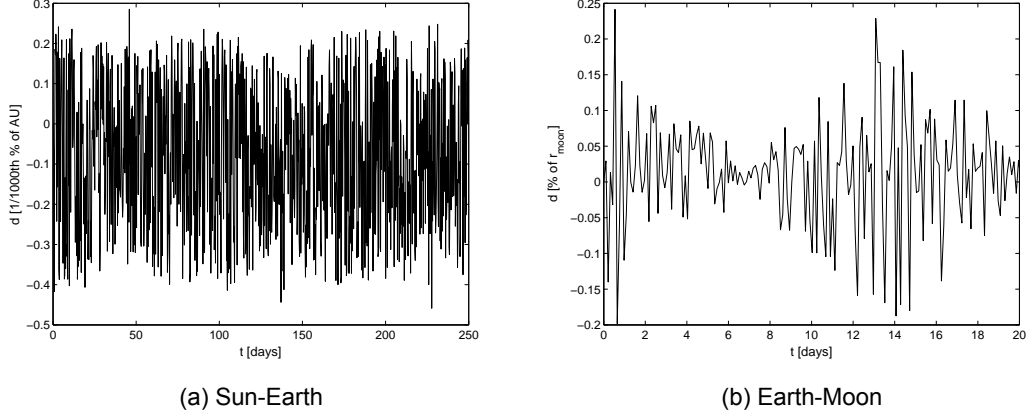


Figure 2.2: Change in distance between the two main bodies, as a fraction of the starting distance

This ephemeris model is a representation of the theory discussed in Section 2.2.1. Due to the foundation of TUDAT, the code can immediately be used to calculate the movement of any spacecraft with given initial conditions.

2.3. Lagrange Libration Points

In the equations of motion of the CR3BP, equilibrium points may be found. These are the Lagrange Points, where the third body can remain in the same position in reference to the two main bodies for a longer period of time. They are essential to manifold orbits, since all the manifold trajectories start or end at an orbit around one of these points. Before we can calculate the locations of low energy trajectories, we must find the locations of the Lagrange points.

2.3.1. Location of the Lagrange Points

The Lagrange points are found on the equilibrium points of the CR3BP, in other words, the places where both the velocity and the acceleration of the third body can be zero. To find these locations, we first look at the places where the velocity is zero, which are called the surfaces of Hill. These can be found by setting an equation for the velocity, Jacobi's integral, to zero.

Jacobi's integral is used to determine the velocity of P3 in the reference frame used for the CR3BP. It is formed by multiplying equation 2.23 with \dot{x} , 2.24 with \dot{y} and 2.25 with \dot{z} , followed by a summation of these equations, to get:

$$\dot{x}\dot{x} + \dot{y}\dot{y} + \dot{z}\dot{z} = \dot{x}\frac{\partial U}{\partial x} + \dot{y}\frac{\partial U}{\partial y} + \dot{z}\frac{\partial U}{\partial z} \quad (2.32)$$

The right side of this equation can be simplified when one realizes that U is only a function of x , y and z , so:

$$\frac{dU}{dt} = \frac{\partial U}{\partial x}\dot{x} + \frac{\partial U}{\partial y}\dot{y} + \frac{\partial U}{\partial z}\dot{z} \quad (2.33)$$

Now, these equations can be combined and integrated to get Jacobi's integral:

$$\dot{x}^2 + \dot{y}^2 + \dot{z}^2 = 2U - C \quad (2.34)$$

Here, C is the integration constant. The right side of the equation is directly related to the definition of velocity V of the particle:

$$V^2 = 2U - C \quad (2.35)$$

The constant C , Jacobi's constant, can be found when combining equation 2.21 and 2.35:

$$C = x^2 + y^2 + \frac{2(1-\mu)}{r_1} + \frac{2\mu}{r_2} + \mu(1-\mu) - V^2 \tag{2.36}$$

Jacobi's constant is the only conserved quantity in the three body problem, and is thus an important description for the state of a spacecraft as it travels under the influence of the two main bodies.

To find the equilibria of the CR3BP, from which useful low energy trajectories originate, we first look at those locations where the velocity of P_3 is zero. The Jacobi's integral and constant are reduced to:

$$2U = C \tag{2.37}$$

$$C = x^2 + y^2 + \frac{2(1-\mu)}{r_1} + \frac{2\mu}{r_2} + \mu(1-\mu) \tag{2.38}$$

Equation 2.38 combined with the equations 2.12 and 2.13, which define r_1 and r_2 , lead to two conclusions. First of all, the surfaces of Hill are symmetric with respect to the XY- and XZ-planes. In the case $\mu = 1/2$, it is also symmetric with respect to the YZ plane. Second, the surface are outwardly bound by a cylinder around the Z-axis, with a radius of \sqrt{C} . This is found when increasing z^2 , which causes an increase in r_1 and r_2 until the limit case $x^2 + y^2 = C$ is reached.

This means that we can determine which areas of the XYZ space can be reached by P_3 , for given initial conditions set in C , as shown in Figure 2.3. The blue regions are called the surfaces of Hill Wakker (2015), and a satellite with the specified energy c cannot reach these regions.

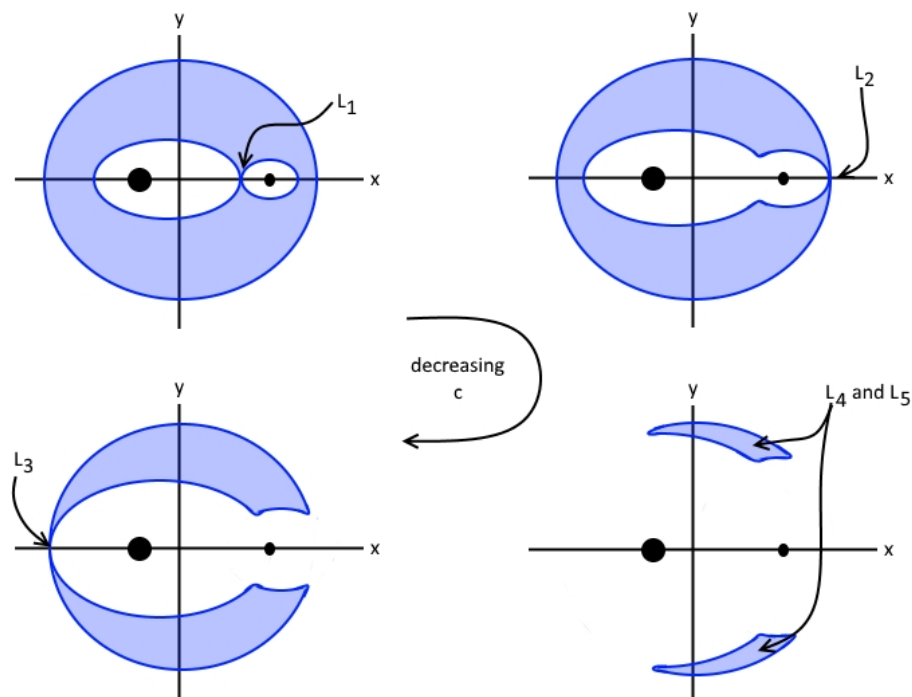


Figure 2.3: Schematic picture of the surfaces of Hill for decreasing values of C . The two black dots on the x-axis are the two main bodies. The blue lines are the outlines of the surfaces of hill. The spacecraft cannot access the blue shaded areas.

The equilibria of the CR3BP are called Lagrange points. Useful low energy trajectories originate from the Lagrange points, and thus it is essential to know how to find these points. Figure 2.3 already shows the Lagrange Points. When C grows, the inaccessible area becomes smaller. At specific times, two parts of the surfaces of Hill touch. This is where the Lagrange points are. Each of the four subfigures

of Figure 2.3 shows a value of C at which a Lagrange point is found.

Equilibria are found when the conditions of the third body are unchanging. Thus, when looking at the equations, the Lagrange points must satisfy the following condition:

$$\frac{\partial U}{\partial x} = \frac{\partial U}{\partial y} = \frac{\partial U}{\partial z} = 0 \quad (2.39)$$

Combining equation 2.39 with 2.18, 2.19, 2.20, 2.23, 2.24 and 2.25 gives:

$$x - \frac{1-\mu}{r_1^3}(\mu+x) + \frac{\mu}{r_2^3}(1-\mu-x) = 0 \quad (2.40)$$

$$y\left(1 - \frac{1-\mu}{r_1^3} - \frac{\mu}{r_2^3}\right) = 0 \quad (2.41)$$

$$z\left(\frac{1-\mu}{r_1^3} + \frac{\mu}{r_2^3}\right) = 0 \quad (2.42)$$

First of all, it must be noted that for all Lagrange points, $z = 0$, because r_1 and r_2 are positive, and $0 < \mu \leq 1/2$. The other two equations lead to the locations of the Lagrange Points, after extensive analytical exploration that shall not be discussed here. For more information, one can for example refer to Wakker (2015). The first three points are on the x -axis. Their location is shown by Figure 2.4 and equations 2.43 through 2.47. The first two equations introduce useful constants, which make for a shorter notation in the last three equations. These last three equations give the values for γ_1 , γ_2 and γ_3 as defined in Figure 2.4.

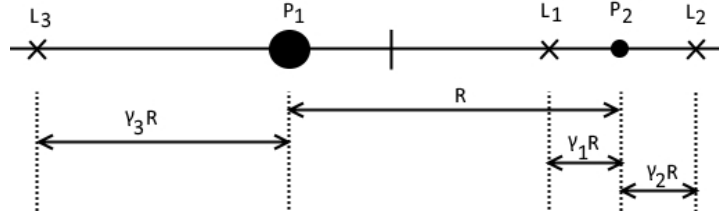


Figure 2.4: Locations of the first three Lagrange Points, relative to the two main bodies, using the variables from equations 2.43 through 2.47.

$$\alpha = \frac{\mu}{1-\mu} \quad (2.43)$$

$$\beta = \left(\frac{1}{3}\alpha\right)^{1/3} \quad (2.44)$$

$$\gamma_1 = \beta - \frac{1}{3}\beta^2 - \frac{1}{9}\beta^3 - \frac{23}{81}\beta^4 + O(\beta^5) \quad (2.45)$$

$$\gamma_2 = \beta + \frac{1}{3}\beta^2 - \frac{1}{9}\beta^3 - \frac{31}{81}\beta^4 + O(\beta^5) \quad (2.46)$$

$$\gamma_3 = 1 - \frac{7}{12}\alpha + \frac{7}{12}\alpha^2 - \frac{13223}{20736}\alpha^3 + O(\alpha^4) \quad (2.47)$$

Where $O(\beta^5)$ and $O(\alpha^4)$ indicates terms of the order β^5 and α^4 respectively, that are emitted from the equation. These terms are small enough to be ignored for most cases.

Lagrange points L_4 and L_5 are found at the following coordinates:

$$x = \frac{1}{2} - \mu \quad (2.48)$$

$$y = \pm \frac{1}{2} \sqrt{3} \quad (2.49)$$

For this research, only the location of L_2 is required, since this is the Lagrange point from which low energy trajectories used for an Earth to Moon transfer originate. From the equations, it can be seen that L_2 moves away from P_2 as the difference in mass between P_1 and P_2 decreases. So, relative to the distance between the two main bodies, the Sun-Earth L_2 point is closer to the Earth than the Earth-Moon L_2 point is to the Moon.

2.3.2. Implementation of the Lagrange Points in TUDAT

The low energy trajectories used in this research all find their origin in the second Lagrange point of either the Sun-Earth system or the Earth-Moon system. Starting positions of the trajectories are found relative to this Lagrange point, as will be explained in Chapter 3. Therefore, the precise location of both the Sun-Earth and Earth-Moon L_2 point must be included in the ephemeris model.

TUDAT already has a script for finding the Libration Points, which uses equations 2.43 through 2.47 with increased series expansions. However, when placing a spacecraft on the location given by these equations in the created ephemeris models, the velocity and acceleration relative to the two main bodies quickly increased, while a spacecraft in a Libration Point should stay still relative to the bodies: The script for finding Libration Points suffers from rounding errors. It was then decided to use minor manual adjustments to the location of the Lagrange points, until the stable location was found. If a spacecraft is placed too far on the positive x-axis, it drifts away from the two main bodies, whereas if it is not placed far enough on the x-axis, it drifts towards the main bodies. This property can be used to locate the correct equilibrium position. This was done as best possible using TUDAT's double-precision floating-point format, which ensured the highest possible precision within the limits of the program. For more information about the written script and the manual adjustments, refer to Appendix A.2.

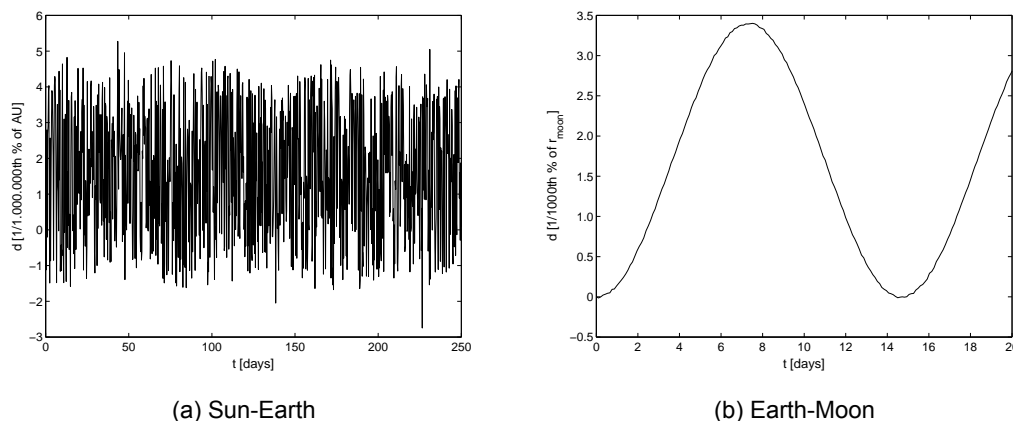


Figure 2.5: Change in distance between the largest of the main bodies and the L_2 point, as a fraction of the starting distance

To verify the model, it was checked if the trajectories are truly circular, by plotting the change in distance between the spacecraft originating in L_2 and the central body. These plots are shown in Figures 2.5a and 2.5b. Note that the timespan of the two plots is different, because it is related to the orbital period of the second body. The Earth-Moon system shows a clear oscillation of one lunar revolution around the Earth. This indicates that the spacecraft origination from the calculated L_2 point follows a slightly elliptical trajectory in the rotating system, instead of the desired circular trajectory with a period equal to that of the Moon. Apart from this, both plots show small, erratic oscillation, which is caused by rounding effects. There is no drift present.

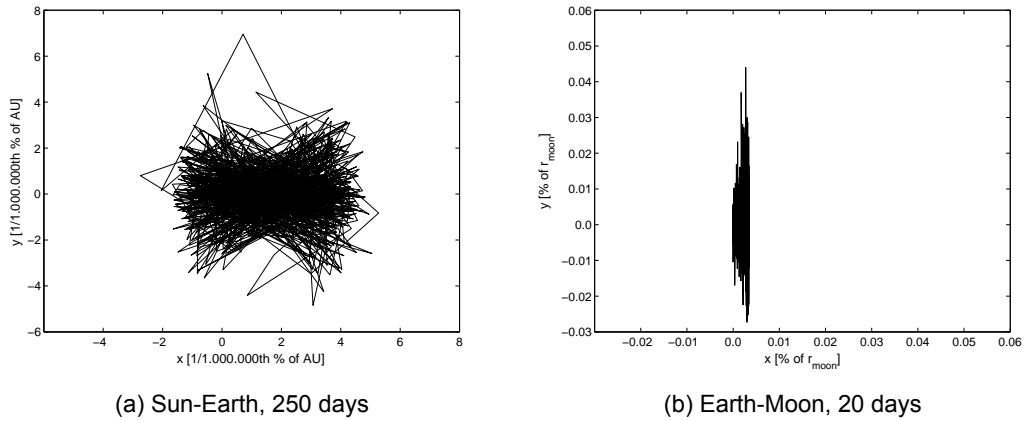


Figure 2.6: Change in location of the L_2 point with respect to the rotating coordinate system of the CR3BP

Additionally, the location of the L_2 point in the rotating system of the CR3BP is plotted in Figures 2.6a and 2.6b. From these plots we can see that the location of the L_2 point is not entirely accurate, and moves with rather erratic behaviour. This fits the expectation of errors due to rounding effects. The divergences remain well within 0.1% of the distances between the main bodies, and spacecraft placed in the L_2 point at the start of the propagation period remain near to this point during the entire propagation. This is the best possible precision while using TUDAT's double-precision floating-point format, and is sufficient according to Howell et al. (2006), where errors up to 0.05% are allowed (p.7). Note that the Earth-Moon L_2 shows different behaviour than the Sun-Earth L_2 . The along-track error of the Earth-Moon L_2 is significantly larger, almost to the limits of the allowed error. This fits with the previous observation that the Earth-Moon L_2 follows a slightly elliptical trajectory in the rotating system: Near the perigee it will move ahead and near the apogee it will stay behind the 'true L_2 ', even though the ellipse itself is only very lightly deviated from a circle.

3

Creating Low Energy Trajectories: Dynamical Systems Theory

The CR3BP creates a model for the problem of an orbit influenced by two major bodies, such as a satellite in the Sun-Earth or Earth-Moon system, as was described in Chapter 2. There are many possible trajectories within the CR3BP. This research focusses on low energy trajectories, which can be found on the invariant manifolds of the CR3BP. Using the theory on low energy trajectories, a database of such trajectories is created. The trajectories in this database will be used as segments for the transfers in Chapter 4.

There is more than one way to find low energy trajectories. Two methods are discussed in detail in literature. The linearised subspace method described by Conley (1968) and Koon et al. (2000b), amongst others, finds a solution to the problem in a linearised subspace. In the solution, several classes of trajectories can be distinguished. The eigenvector method described by Guzman et al. (1998) and Topputo et al. (2005), amongst others, uses the eigenvectors of the problem to describe a vector offset. It allows for the creation of homoclinical and heteroclinical connections (van der Ham, 2012).

For this research it is necessary to study different classes of low energy trajectories, because combinations of such classes lead to the possible configurations which are compared. Therefore, it is essential to choose a method which is capable of finding low energy trajectories per specified class. The eigenvector method has no simple way to do so. For this reason, it was chosen to use the linearised subspace method, which is based on nine classes within four categories. These classes provide possible combinations leading to the four configurations specified by the sub-questions of this research.

The linearised subspace method of finding invariant manifolds consists of a few steps. The first step is the linearisation of the non-linear system of equations. For low energy trajectories, this linearisation is performed at the location of the Lagrange points, where the different classes of invariant manifolds of the CR3BP come together. The second step is to find the eigenvectors of the linearised problem, and use these as the axis of the subspace. This results in the equations of motion within the subspaces. As the third step, these equations are studied to find classes of solutions. These solutions are the initial conditions of trajectories in the invariant manifolds. The fourth step is to translate the initial conditions of the found classes of solutions back into the original solution space, to get the initial conditions of low energy trajectories in the linearised system. These initial conditions can then be integrated in the CR3BP to find the full trajectories.

3.1. Linearisation of the CR3BP

The first step in finding the invariant manifolds of the CR3BP is the linearisation of the CR3BP near the co-linear Lagrange libration points (Koon et al., 2000b). In the coordinate system of the CR3BP, the co-linear Lagrange point has coordinates $(k, 0)$. For the linearisation, we change the coordinate system to have the origin in the Lagrange point. The direction of the axis remains unchanged. The quadratic terms

of Hamiltonian equation 2.26 as expanded over the equilibrium point in the new coordinate system are used to get the linearised Hamiltonian equation:

$$H_l = \frac{1}{2} [(p_x + y)^2 + (p_y - x)^2 - ax^2 + by^2] \quad (3.1)$$

As before, x and y are the coordinates of a particle and p_x and p_y are the momentum variables in the direction of the x -axis and the y -axis. The axes have the same directions as those of the CR3BP, but the origin is moved to the equilibrium point. Variables a and b were introduced to keep the equation readable:

$$a = 2\rho + 1 \quad (3.2)$$

$$b = \rho - 1 \quad (3.3)$$

For simplicity, both use the variable ρ , defined as:

$$\rho = \mu(k - 1 + \mu)^{-3} + (1 - \mu)(k + \mu)^{-3} \quad (3.4)$$

The variable μ again is the mass variable defined as $m_2/(m_1 + m_2)$ and k is the x -coordinate in the CR3BP of the Lagrange point around which the linearisation is performed. The variable ρ is thus different for each of the Lagrange points, meaning that the Hamiltonian is different for each of the Lagrange points. This will eventually result in differences in the path the low energy trajectories follow. Nonetheless, the method remains the same for each of the three co-linear Lagrange points.

From the linearised Hamiltonian around the Lagrange point, the following system of linearised equations is created:

$$\dot{x} = \frac{\delta H}{\delta p_x} = p_x + y \quad (3.5)$$

$$\dot{y} = \frac{\delta H}{\delta p_y} = p_y - x \quad (3.6)$$

$$\dot{p}_x = -\frac{\delta H}{\delta x} = p_y - x + ax \quad (3.7)$$

$$\dot{p}_y = -\frac{\delta H}{\delta y} = -p_x - y - by \quad (3.8)$$

However, computations can be simplified by a transformation from the momenta to the velocities in the rotating system with $v_x = p_x + y$ and $v_y = p_y - x$. This gives the following linearised system to describe the CR3BP near the co-linear Lagrange points:

$$\dot{x} = v_x \quad (3.9)$$

$$\dot{y} = v_y \quad (3.10)$$

$$\dot{v}_x = 2v_y + ax \quad (3.11)$$

$$\dot{v}_y = -2v_x - by \quad (3.12)$$

Note that the Hamiltonian is directly related to the Jacobi constant through equations 2.26 and 2.38, and that the energy level of the particle travelling through the system can thus be chosen by determining the value for H . We may also take the integral of the Hamiltonian:

$$E_l = \frac{1}{2}(v_x^2 + v_y^2 - ax^2 + by^2) \quad (3.13)$$

This is the energy integral of the Hamiltonian, which is also related to the Jacobi constant. When we wish to consider the Hamiltonian as a function of position and velocity, we may use E , while we use H when we consider a function of position and momentum.

3.2. Transformation of CR3BP to Subspaces

Invariant manifolds can be found in the subspaces defined by the eigenvectors of a system of equations. The eigenvectors become the new axes of the coordinate system, and the equations of motion are rewritten to match to these axes. Then, solutions to these equations of motion may be found.

From the system of equations of the linearised system, equation 3.9 through 3.12, the eigenvalues can be found through linear algebra (Lay, 1994). The eigenvalues of the linearised system are of the form $\lambda_1 = \lambda$, $\lambda_2 = -\lambda$, $\lambda_3 = iv$ and $\lambda_4 = -iv$, where λ and v are positive constants dependent on the variables in the Hamiltonian, and $i = \sqrt{-1}$ (Koon et al., 2000b). Through linear algebra, the eigenvalues lead to the eigenvectors. For this, two constants σ and τ are introduced, which may be positive or negative. This leads to the four eigenvectors u_1 , u_2 , w_1 and w_2 in x , y , v_x , v_y coordinates:

$$u_1 = \begin{bmatrix} 1 \\ -\sigma \\ \lambda \\ -\lambda\sigma \end{bmatrix}$$

$$u_2 = \begin{bmatrix} 1 \\ \sigma \\ -\lambda \\ -\lambda\sigma \end{bmatrix}$$

$$w_1 = \begin{bmatrix} 1 \\ -i\tau \\ iv \\ v\tau \end{bmatrix}$$

$$w_2 = \begin{bmatrix} 1 \\ i\tau \\ -iv \\ v\tau \end{bmatrix}$$

Like the eigenvalues, the eigenvectors change dependent on the variables in the Hamiltonian. These are dependent on the system that is used (Sun-Earth, Earth-Moon, etc.) and on which of the co-linear Lagrange points is currently considered.

The subspace in which the invariant manifolds are situated can now be created, with the eigenvectors as the new axes. To make clear difference between the coordinates of the CR3BP and of the subspace, we do not use variables which were used before such as x and y for the subspace. Instead, we use as coordinates ξ for the u_1 axis, η for the u_2 axis, ζ_1 for the w_1 axis and ζ_2 for the w_2 axis. Equations 3.9 through 3.12 are rewritten to fit to the new coordinate system. This gives the following differential equations:

$$\dot{\xi} = \lambda\xi \tag{3.14}$$

$$\dot{\eta} = -\lambda\eta \tag{3.15}$$

$$\dot{\zeta}_1 = v\zeta_2 \tag{3.16}$$

$$\dot{\zeta}_2 = -v\zeta_1 \tag{3.17}$$

Additionally, the energy integral of the Hamiltonian, equation 3.13 can be rewritten into the new coordinate system:

$$E = \lambda\xi\eta + \frac{v}{2}(\zeta_1^2 + \zeta_2^2) \tag{3.18}$$

Note that this new set of differential equations in the transformed coordinate system is simpler than the original set of equations in the linearised CR3BP. This is exactly the purpose of the transformation: The equations are rewritten in a simpler set of differential equations, of which a solution may be found.

The solution of this system of differential equations, in the form of trajectories through the subspace, can be described as follows, using initial conditions ξ^0 , η^0 and $\zeta^0 = \zeta_1^0 + i\zeta_2^0$ (Boyce and DiPrima, 2010):

$$\xi(t) = \xi^0 e^{\lambda t} \quad (3.19)$$

$$\eta(t) = \eta^0 e^{-\lambda t} \quad (3.20)$$

$$\zeta(t) = \zeta_1(t) + i\zeta_2(t) = \zeta^0 e^{-i\nu t} \quad (3.21)$$

This describes the subspace of the invariant manifold. Note that E from equation 3.18 should be constant, and therefore the functions $\eta\xi$ and $|\zeta|^2 = \zeta_1^2 + \zeta_2^2$ must be constant along solutions.

The solution of the differential equations of the linearised problems in this manifold are possible trajectories for a spacecraft where no burns are needed. It is now possible to classify the possible trajectories into groups, to make further study of the trajectories through invariant manifolds easier.

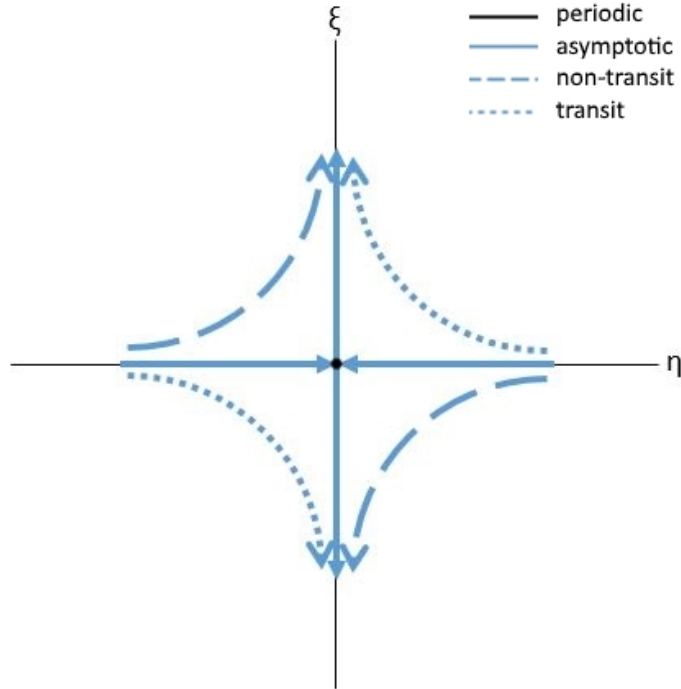


Figure 3.1: The nine classes of trajectory on the ξ - η plane. The origin is the Lagrange Point. The first class is the periodic orbit, where $\eta = \xi = 0$, which is seen here as a dot in the origin. The second, third, fourth and fifth class are asymptotic trajectories, where $\eta\xi = 0$, shown by the solid arrows on the axis. The sixth and seventh class are transit trajectories, where $\eta\xi > 0$, shown by the dotted arrows in the left bottom and right top. The eighth and ninth class are non-transit trajectories, where $\eta\xi < 0$, shown by the dashed arrows in the left top and right bottom.

3.3. Classes of Trajectories in the Subspaces

To find the invariant manifolds which are relevant to the problem, we look at the projection of several trajectories on the ξ - η plane. Because there are no burns in the trajectories of interest, we know that the Hamiltonian function (equation 3.18) must remain constant, so $\eta\xi$ is constant, and $|\zeta|^2 = \zeta_1^2 + \zeta_2^2$ is constant. Using this, Koon et al. (2000b) describes 9 different classes of trajectories found in Equations

3.19 through 3.21, divided into four categories. For each of the found classes, we know that the ζ plane describes only circles.

1. $\eta = 0$ and $\xi = 0$. The black dot in the origin of the plane of Figure 3.1 is the **periodic** solution. In the subspace, a spacecraft can be at rest in this point.
2. $\eta\xi = 0$. The full arrows in Figure 3.1 indicate the four classes of **asymptotic** trajectories. For $\xi = 0$, they are asymptotic towards the centre of the coordinate system for increasing time, and for $\eta = 0$ they are asymptotic towards the origin of the coordinate system for decreasing time.
3. $\eta\xi = c > 0$. The dotted arrows in Figure 3.1 indicate two classes of **transit** trajectories. In the subspace they first approach the origin of the coordinate system along the η axis, then move away again along the ξ axis.
4. $\eta\xi = c < 0$. The dashed arrows in Figure 3.1 indicate the two classes of **non-transit** trajectories. In the subspace they behave similarly to the transit trajectories, but in different segments. They first approach the origin of the coordinate system along the η axis, then move away again along the ξ axis.

Note that the four categories together form a saddle point around the origin of the subspace.

3.4. Classes of Trajectories in the CR3BP

The projection of the four categories of trajectories on the ξ - η plane is not sufficient for designing low energy trajectories. Equations 3.19 through 3.21 must be transformed back from the subspaces, into the x , y , v_x , v_y coordinates of the CR3BP. Conley (1968) shows that a system of equations with eigenvalues λ , $-\lambda$, iv and $-iv$, and with eigenvectors u_1 , u_2 , w_1 and w_2 , has the following general, real solution:

$$\begin{bmatrix} x(t) \\ y(t) \\ \dot{x}(t) \\ \dot{y}(t) \end{bmatrix} = \alpha_1 e^{\lambda t} \begin{bmatrix} 1 \\ -\sigma \\ \lambda \\ -\lambda\sigma \end{bmatrix} + \alpha_2 e^{-\lambda t} \begin{bmatrix} 1 \\ \sigma \\ -\lambda \\ -\lambda\sigma \end{bmatrix} + 2\Re(\beta e^{ivt} \begin{bmatrix} 1 \\ -i\tau \\ iv \\ v\tau \end{bmatrix}) = \alpha_1 e^{\lambda t} u_1 + \alpha_2 e^{-\lambda t} u_2 + 2\Re(\beta e^{ivt} w_1) \quad (3.22)$$

Note that this equation is very similar to a combination of equations 3.19 through 3.21. They are essentially the same, but in different reference frames. Also note that α_1 and α_2 are real constants, and β is a complex constant. We can vary the values of α_1 and α_2 , to get the same nine classes as were defined in the subspace. The value of β has no effect on the class, but it does influence the energy level of the trajectory.

1. The **periodic** orbit is found when $\alpha_1 = \alpha_2 = 0$. It is shown as the black ellipse around the centre Figure 3.2: A Lyapunov Orbit. It can be shown that the size of the ellipse is set Conley (1968): The major axis has a length of $2\tau\sqrt{H_l/\kappa}$ and the minor axis has a length of $2\sqrt{H_l/\kappa}$, where H_l is the Hamiltonian, and constant $\kappa = -a + b\tau^2 + v^2 + v^2\tau^2$. Here, a and b are the variables defined by Equations 3.2 and 3.3, and τ and v where defined in the eigenvectors. Thus, as the Hamiltonian function (and thus the energy) increases, the ellipse grows.
2. The **asymptotic** trajectories are found for $\alpha_1\alpha_2 = 0$. They are shown by the full, blue, spiralling trajectory in Figure 3.2. A distinction can be made between trajectories with $\alpha_1 = 0$, which are bound by the lines

$$y = \sigma x \pm 2\sqrt{H_l(\sigma^2\tau^2)/\kappa} \quad (3.23)$$

and the trajectories with $\alpha_2 = 0$, which are bounded by the lines

$$y = -\sigma x \pm 2\sqrt{H_l(\sigma^2\tau^2)/\kappa} \quad (3.24)$$

Here, σ and τ are the values that were found in the eigenvector, H_l is the Hamiltonian and κ was defined in the first category of trajectories. These strips are shown in grey in Figure 3.2 and touch on the periodic orbit.

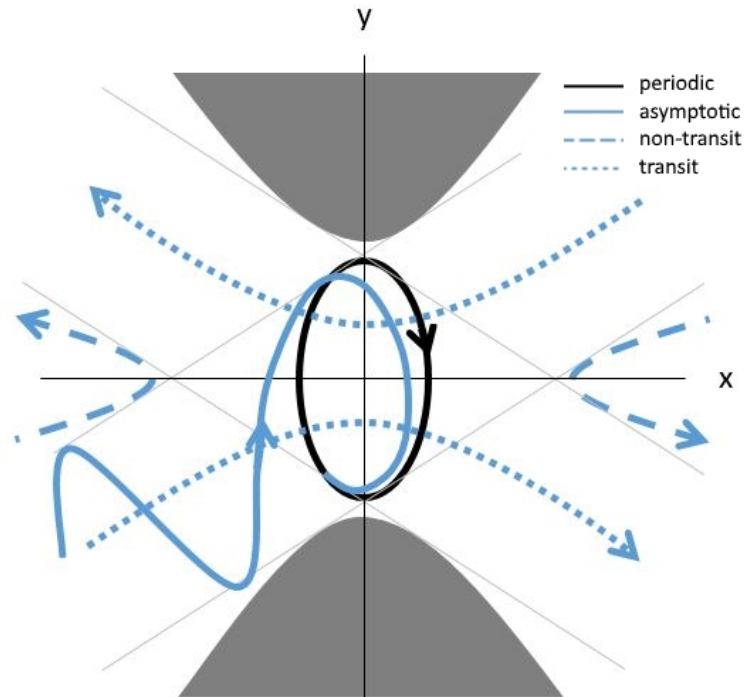


Figure 3.2: The nine classes of trajectories on the xy plane. The grey areas are the surfaces of Hill. The origin is the Lagrange Point. The first class is the periodic orbit, where $\alpha_1 = \alpha_2 = 0$, which is seen here as a black ellipse around the origin. The second, third, fourth and fifth class are asymptotic trajectories, where $\alpha_1 \alpha_2 = 0$. For clarity, only one is shown by the solid spiralling blue arrow on the axis. In reality, there would be one spiralling arrow in each of the four quadrants. The sixth and seventh class are transit trajectories, where $\alpha_1 \alpha_2 < 0$, shown by the dotted blue arrows. The eighth and ninth class are non-transit trajectories, where $\alpha_1 \alpha_2 > 0$, shown by the dashed blue arrows in the left top and right bottom. The four grey lines are determined by Equations 3.23 and 3.24.

3. The **transit** trajectories are found for $\alpha_1 \alpha_2 < 0$. They are shown by the dotted, blue trajectories in Figure 3.2. They transit from the inner regions of the surfaces of Hill to the outer region or vice versa.
4. The **non-transit** trajectories are found for $\alpha_1 \alpha_2 > 0$. They are shown by the dashed, blue trajectories in Figure 3.2. They stay on one side of the surfaces of Hill.

Note that all these trajectories are found in the linearised space around the Lagrange point, and are therefore only reliable near these points. Therefore, equation 3.22 can be used to find initial conditions near the Lagrange point, from which the path should be propagated to get the full trajectory.

3.5. Implementation of trajectories in TUDAT

This research will use the different classes of low energy trajectories to create different configurations for a transfer. As described above, these trajectories are created using initial conditions in the vicinity of the Lagrange Libration points. In order to create the database of trajectories that is necessary for this research, the TUDAT script discussed in Section 2.3.2 was expanded to allow the creation of low energy trajectories in each of the nine classes. This script has two main parts: The initial condition creation and the propagation of the trajectory.

The creation of initial conditions for each of the nine classes is done using equation 3.22. As described in Section 3.4, the value for α_1 and α_2 decides in which of the classes the trajectory belongs. Varying the value of t changes the location at which the trajectory starts. β can also be varied to get different sets of initial conditions for the specified class. The choice of possible values for α_1 , α_2 , β and t consists of three steps: First the minima and maxima for each variable are found. Then the sampling interval

is chosen. Lastly, a check is performed to see if the resulting initial conditions are within the allowed energy range. The used variables can be found in Appendix A.3. The process will be described in more detail below.

The first variable for which the minimum and maximum value are determined is t . Here, the values should be chosen in such a way that a full revolution of the periodic orbit is passed. When this full revolution is passed, higher values of t will give the same results. The minimum value of t is always set to zero. The maximum value was found through experimentation on initial conditions for the periodic orbit. Here, $\alpha_1 = \alpha_2 = 0$. Through manual experimentation it was found that the value of t at which a full revolution of the periodic orbit is past, is not dependent on β . Through this method the maximum required value for t is found. The value is then rounded up to an integer. This is done for two reasons: First of all, it ensures that the entire range is indeed used, and not shortened by rounding errors and such. Secondly, it ensures that no matter what the sampling interval will be, it will not be exactly mirrored over the periodic ellipse. This is beneficial because it ensures there is a larger variety in the resulting trajectories.

To determine the minimum and maximum values for α_1 , α_2 and β , the allowed energy levels must be considered. For this research, only energy levels are allowed at which the Hill-sphere has already opened at L_2 but not yet at L_3 (see Figure 2.3). Trajectories with energy levels where the Hill-sphere has not yet opened at L_2 are not useful for this research, because the research focusses on the low energy trajectories on the L_2 manifold. Trajectories with energy levels where the Hill-sphere has already opened at L_3 move at such distances from the main body or at such high speeds that it is not possible to create a link between the Sun-Earth and Earth-Moon segments of the transfers.

The second variable for which the minimum and maximum value are determined is β . Again, the periodic solution is used, where $\alpha_1 = \alpha_2 = 0$. First, the minimum value for β is determined. Starting from $\beta = 0$ and moving down with steps of $0.5 * 10^{-2}$, the initial conditions for that value of β and three values of t are calculated. The values of t are the minimum value, the maximum value, and the value exactly in-between. When this is done, the energy level of these initial conditions are calculated using equation 2.38. When each of the energy levels falls outside of the allowed range, the current value of β is set as the minimum. All higher values fall within the energy levels. The same is then done for the maximum value, but instead of moving down steps from $\beta = 0$, steps of the same size are moved up. This results in a minimum and maximum value of β .

The process for finding minimum and maximum values for α_1 and α_2 work in similar ways. For α_1 unstable asymptotic trajectories are used, where $\alpha_2 = 0$. For α_2 stable asymptotic trajectories are used, for which $\alpha_1 = 0$. For both β and t the minimum, maximum and the value exactly in between are used. Moving away from $\alpha_1 = 0$ or $\alpha_2 = 0$ with a step-size of $0.5 * 10^{-2}$ again, the initial conditions and their associated energies are calculated. The first value for α_1 or α_2 for which all initial conditions fall without the allowed energy range are the minimum and maximum.

Having found the initial conditions, the sampling size for each of the variables must be chosen. The sampling size has effect on the number of trajectories that are found. The research would benefit from a large set of trajectories, and as such the sampling size should be large. However, a larger sampling size results in longer computation times. Therefore, the sampling size is limited by the scheduled running time for the trajectory creation script. From manual experimentation it was found that a large sample size for β has more variety in trajectories as a result than a large sample size for the other variables. As such, it was decided that β would have a sample size four times larger than the other variables. Using this decision, the sample size for each of the variables was manually varied to find the sample size resulting in the largest set possible within allowed running times for the scripts. The resulting values for the variables are found in Appendix A.3.

Having created sampling sets for each of the variables, a complete set of initial conditions can be created. At this point it is important to perform an additional check on the energy levels, because certain combinations on variables may result in initial conditions which do not fit within the allowed ranges. As such, for every initial condition found, the energy is again calculated using Equation 2.38. Initial conditions with energies out of the allowed ranges are then discarded.

Initial conditions are created per trajectory class. When the initial conditions of one trajectory class are created, the trajectories can be propagated, using scripts build into TUDAT. Using a variable step size Runge-Kutta-Fehlberg-78 integrator and Cowell propagator, the initial conditions are propagated in the CR3BP (Fehlberg, 1969). Dependent on the class of the initial conditions, this is either a backwards or a forwards propagation. For the transit and non-transit trajectories, each of the initial conditions was propagated in both directions. The propagated trajectories are then written to a file. In order to limit the amount of space used, only 1000 states of each trajectory are saved, linearly distributed over the original states. This means that in the places that had a smaller time-step due to the variable step size integration, more states will still be saved. The files are each given a name which includes the trajectory class, and the values of α_1 , α_2 , β and t , so the initial conditions may be reproduced.

Using this script, it is possible to create a database of trajectories, divided over the different classes of trajectories. The only class of trajectory that is not created is the periodic orbit, since these are not used for the different configurations of transfers. For more details about the script, refer to Appendix A.

The final database includes over 4000 trajectories per class of trajectories in the Sun-Earth system, and over 400 trajectories per class of trajectories in the Earth-Moon system. The choice was made to use less trajectories in the Earth-Moon system, since these trajectories will later be plotted at several angles due to the rotation of the Moon, and a larger number of used trajectories would slow down the code too significantly. This is further discussed in Chapter 4. The question of whether these numbers of trajectories are sufficient to create a robust transfer creation script is discussed in Section 5.5, where a test is performed to see if the results would be the same with less trajectories available.

Unfortunately the linear subspace method as described by Conley (1968) is used rarely in research, since other methods are more favourable for, amongst others, computation time, and many types of research do not need the classification of trajectories. Because of this, there are no example trajectories found which are created using this methodology, which makes the validation of the resulting trajectories difficult. What can be done is a visual comparison of each class of trajectories with visual sources from literature. Sources such as Conley (1968), Koon et al. (2001) and Koon et al. (1999) have figures depicting the trajectory classes, which show that the results from the propagation are at least visually the same, and that the initial conditions created per trajectory class also deliver trajectories of this class only.

This, of course, is not sufficient validation of the trajectories. As an additional validation, the first sub-question of the research is used. This combines non-transit trajectories in the Sun-Earth system with stable asymptotic trajectories in the Earth-Moon system. Koon et al. (2001) describes the creation of such a transfer and shows their ideal transfer. In Chapter 5 their solution will be compared with the solution found from the trajectory database, to further validate the database.

4

Creating Low Energy Transfers: Trajectory Linking

Having created a database of trajectories as described in Chapter 3, the next step of the research is to create transfers from the vicinity of the Earth to the Earth-Moon L_2 Lagrange point. This is done using four different configurations, as described by the sub-questions of the research:

1. What is the range for ΔV and transfer time, for the 'standard' ballistic transfer?
2. What is the range for ΔV and transfer time, for the ballistic transfer, when the location of the transfer from the first section to the second section is allowed to vary?
3. What is the range for ΔV and transfer time, for a non-ballistic transfer with three segments (Earth - Sun-Earth L_2 , Sun-Earth L_2 - Moon influence, Moon influence - Earth-Moon L_2)?
4. What is the range for ΔV and transfer time, for a non-ballistic transfer with up to five burns in unspecified locations?

Each of the four configurations are discussed in here. The resulting transfers are discussed in Chapter 5.

4.1. Standard approach

The standard approach is considered the validation approach. It follows a similar configuration as described by Koon et al. (2001), which is a simplified version of the transfer the Hiten mission used (Uesugi et al., 1991). The Hiten mission has the closest similarity of all flown missions to the mission that is discussed in this thesis. The main difference is the desired final state. Where we research a mission which ends in an elliptic orbit around the Earth-Moon L_2 Lagrange point, the Hiten mission was intended to end in an orbit around the Moon, in which it should be ballistically captured. Unfortunately, there have been no missions to the Earth-Moon L_2 using low energy trajectories, nor has there been much research into such missions. Therefore, the Hiten mission is our go-to mission for verification purposes.

The standard approach consists of two segments. The first segment is a non-transit trajectory on the inside of the Hill-sphere in the Sun-Earth system, and the second segment is a stable asymptotic trajectory outside of the Hill-sphere of the Earth-Moon system. Traditionally, the link between these two segments is placed on a line through Earth and perpendicular to the axis on which the Sun and Earth move. This line where the trajectories link is called the Poincaré cut. A schematic overview of the standard approach is shown in Figure 4.1.

To find standard approach transfers, the crossing with the Poincaré cut (positive y-axis) of all Sun-Earth non-transit trajectories inside the Hill-sphere are compared with the crossing with the Poincaré cut of all Earth-Moon stable asymptotic trajectories outside of the Hill-sphere. Because the trajectories are

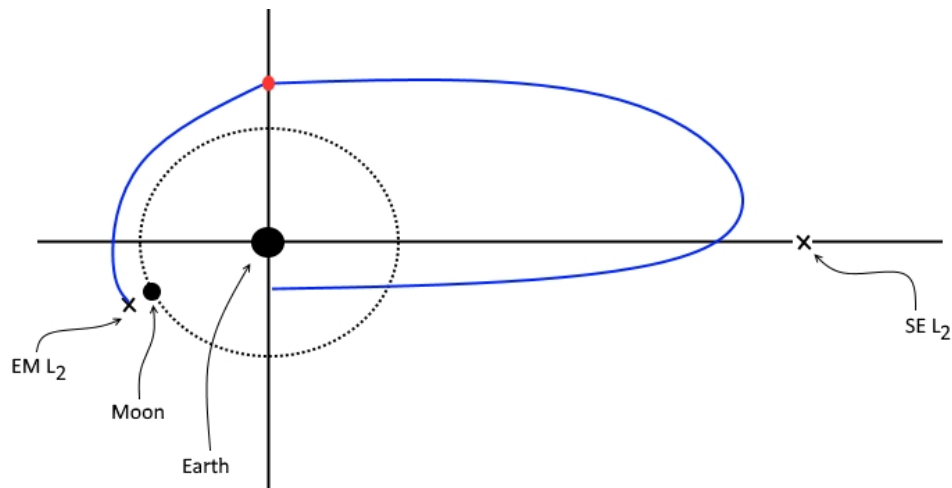


Figure 4.1: A schematic overview of the standard approach. The blue lines are the transfer trajectory that is followed. The red dots are links between segments, where a burn is required.

saved as a collection of 1000 state vectors, it is unlikely that each trajectory has a state vector exactly on the Poincaré cut. Therefore, for each trajectory, the last vector before and the first vector after the Poincaré cut are located. A line is drawn between these two points, on which both position and velocity are assumed to change linearly. The timespan between two points is less than five minutes, and the links are made in regions far from the L_2 point, so the motion here is stable and not chaotic. The position error of the link was found to be less than 5% of the distance between the two points. The lines between the points are then used to find intersections of the first and second segment of the transfer. If an intersection between two trajectories is found, a standard approach transfer is constructed.

4.2. Three asymptotic segments

The first diversion from the standard approach uses three asymptotic segments. The first two segments are similar to the trajectory followed by the Genesis mission (Koon et al., 1999), or researched by (Barden et al., 1996) and (Mingotti et al., 2010). The third segment is somewhat similar to the research by (Koon et al., 2000a), although they do research for Jovian Moons instead of the Earth's Moon.

The first segment is a stable asymptotic trajectory on the inside of the Hill-sphere in the Sun-Earth system, the second segment is an unstable asymptotic trajectory on the inside of the Hill-sphere in the Sun-Earth system and the third segment is a stable asymptotic trajectory outside of the Hill-sphere of the Earth-Moon system. The link between the first two segments is on the elliptical orbit around the L_2 point. The link between the last two segments is the same as for the standard approach: On the Poincaré cut. A schematic overview of the three asymptotic segments approach is shown in Figure 4.2.

The benefit of using three segments is the time that can be spent in orbit around the Sun-Earth L_2 point. The asymptotic trajectories automatically converge to an elliptic orbit around this point, and the amount of ΔV required to leave it again does not change with the time spent there. This allows for additional mission objectives which can be performed at this point. Also, it allows for a station-keeping orbit which makes the scheduling of the transfer far easier. Without this station-keeping orbit, a launch delay of a day will result in a changed transfer trajectory, because the Moon would have moved away from the desired arrival location. With a station-keeping orbit, a delay of a day does not need to mean any change in transfer trajectory at all, it only means that a delay will occur while the satellite stays in orbit around the L_2 point, waiting for the Moon to be in the ideal position again.

To find transfers using the three asymptotic segments approach, all possible links between the first two segments are first computed. The entire trajectories are compared to establish if an intersection exists. If only one intersection exists for a specific combination of trajectories, this link is saved. If multiple intersections exist, the ΔV needed to perform this link is checked. Only the link which requires the

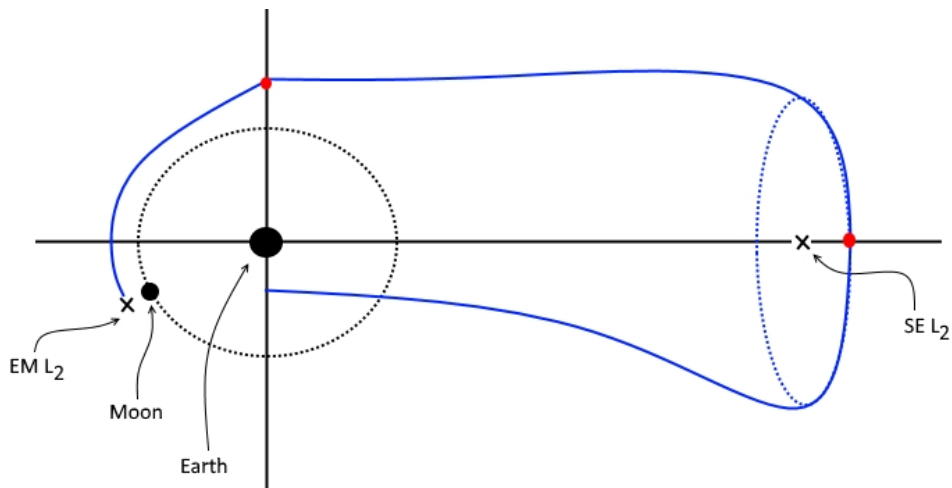


Figure 4.2: A schematic overview of the three asymptotic segments approach. The blue lines are the transfer trajectory that is followed. The red dots are links between segments, where a burn is required.

least ΔV is saved. For each saved link, then, the intersection with the third segment is searched. This happens in the same manner as for the standard approach. When two consecutive intersections between the three trajectories are found, a three asymptotic segment transfer is constructed.

4.3. Free location of linking

The second diversion from the standard approach has the same two segments, but does not use the Poincaré cut as the link location. Instead, this location is left free, and can be different for each transfer option. This diversion has been researched for low energy trajectories which are completely in the Sun-Earth system (Langemeijer, 2018) and proven more beneficial than using the standard Poincaré cut. However, no such research has yet been performed for low energy trajectories to the Moon. A schematic overview of the free linking approach is shown in Figure 4.3.

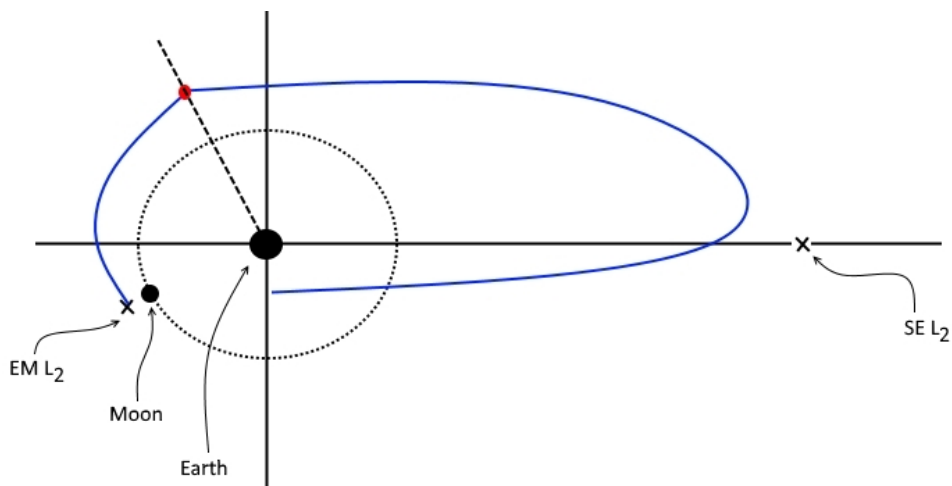


Figure 4.3: A schematic overview of the free linking approach. The blue lines are the transfer trajectory that is followed. The red dots are links between segments, where a burn is required. The dashed line is the new location of the Poincaré cut.

To find free linking approach transfers, the entire trajectories of all Sun-Earth non-transit trajectories inside the Hill-sphere are compared with the entire trajectories of all Earth-Moon stable asymptotic trajectories outside of the Hill-sphere. With this method, any angle between the Poincaré cut and the y-axis is allowed. If only one intersection exists for a specific combination of trajectories, this link is

saved. If multiple intersections exist, the ΔV needed to perform this link is checked. Only the link which requires the least ΔV is saved. If an intersection between two trajectories is found, a free linking approach transfer is constructed.

4.4. All classes, all link locations

The third diversion from the standard approach is chosen to take away as many of the limitations of this approach as possible. The classes of trajectories that are used are not limited, with the exception of using a stable asymptotic trajectory outside of the Hill-Sphere in the Earth-Moon system as the last segment of the transfer, which is necessary to arrive in an orbit around the Earth-Moon L_2 Lagrange point. The number of segments is not pre-defined, although the limit is set to six segments to limit the computation time. There is no literature on using low energy trajectories in this way. A schematic overview of the limitless approach is shown in Figure 4.4.

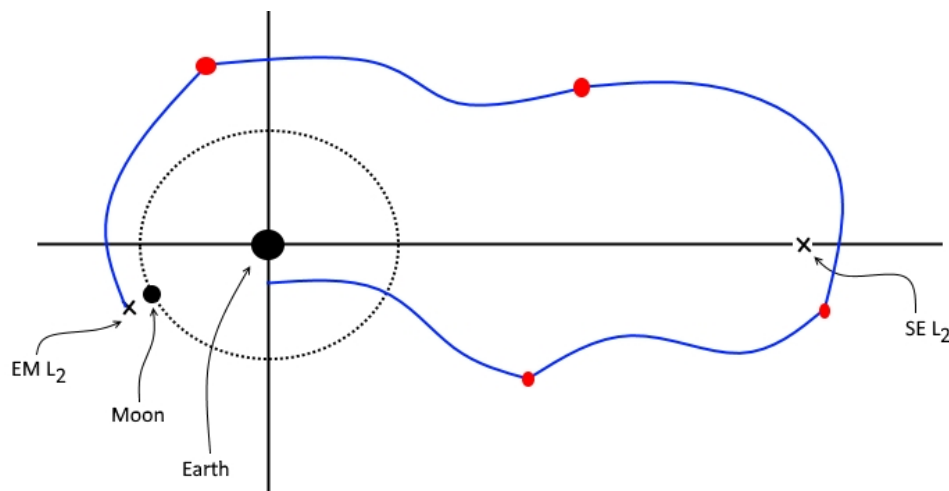


Figure 4.4: A schematic overview of the limitless approach. The blue lines are the transfer trajectory that is followed. The red dots are links between segments, where a burn is required.

The method to find transfers with the limitless approach is quite different from the approaches used before. To start with, all the trajectories are compared to each other, to find all the possible links. All links with a ΔV above 50 m/s are discarded, since they will not result in transfers with a sufficiently low ΔV to compete with transfers from other approaches. Using the resulting set of links, a branching approach is used to find transfers. To clarify the branching method, a simplified visualisation is shown in Figure 4.5. In this image, each arrow is a representation of a trajectory. The desired starting location of the transfer is shown on the left, the desired destination on the right. The branching approach works in several steps:

1. Identify all trajectories that pass through the desired starting location. In Figure 4.5.1 these are shown in red. In the case of real trajectories, these are trajectories that pass along the negative y-axis of the CR3BP while travelling in the direction of the positive x-axis.
2. For each of the trajectories found in step 1, perform steps 3 through 17. Name the currently chosen trajectory the 'starting segment'. The starting segment chosen in the simplified figures is shown in blue in Figure 4.5.2.
3. Find all the trajectories that cross the path of the starting segment. These trajectories are shown in red in Figure 4.5.2.
4. For each of the trajectories found in step 3, perform steps 5 through 17. Name the currently chosen trajectory the 'second segment'. The starting segment and second segment chosen in the simplified figures are shown in blue in Figure 4.5.3.

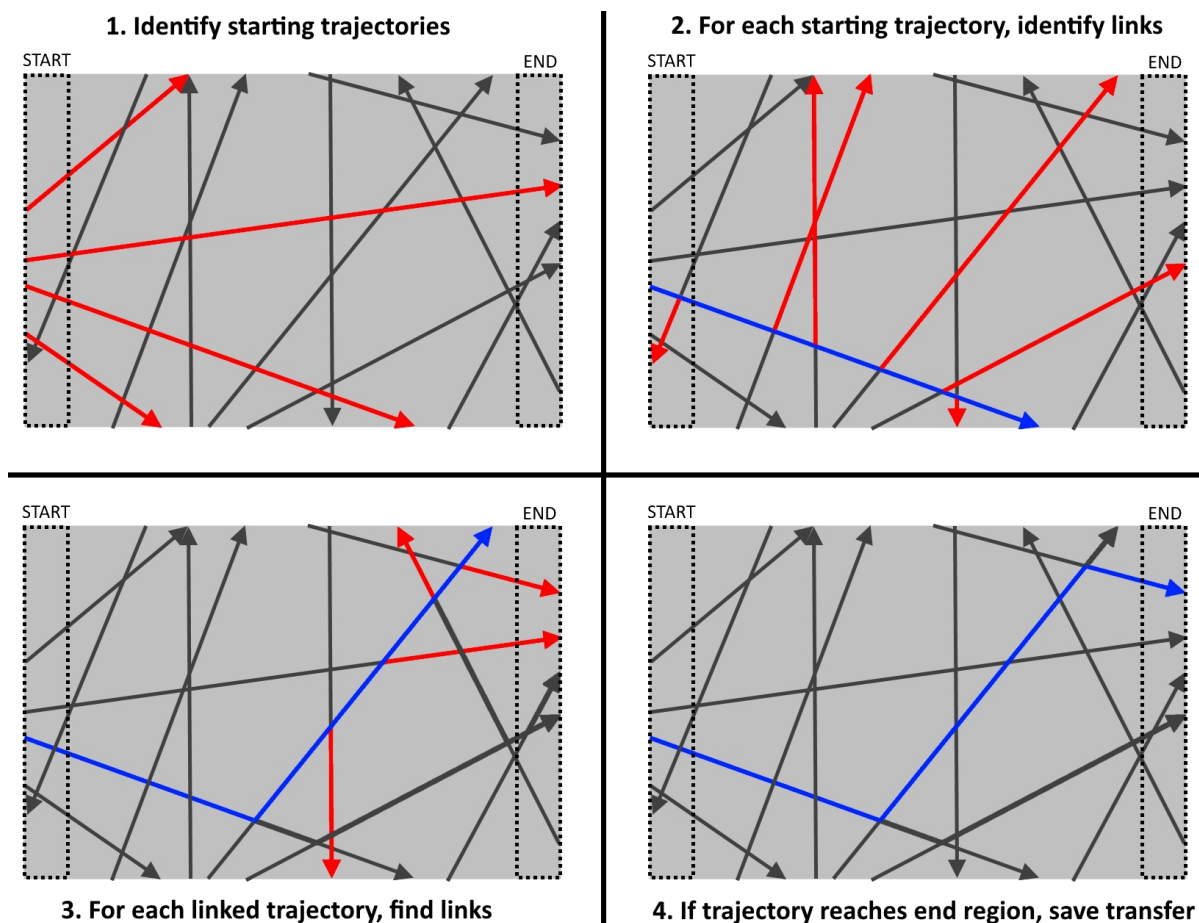


Figure 4.5: Schematic overview of the branching method, as described in steps one through eight of the numbered list.

5. Check if the desired ending criteria are met. In the simplified figures, this would happen if the second segment passed through the end region. Note that this is not the case. In the case of real situations, this would happen if the second segment is a stable asymptotic trajectory outside of the Hill-Sphere of the Earth-Moon system. If the criteria are met, the transfer is saved and the script returns to the next trajectory of step 4. Otherwise, the script continues with step 6.
6. Find all the trajectories that cross the path of the second segment after it has crossed the starting segment. These trajectories are shown in red in Figure 4.5.3.
7. For each of the trajectories found in step 6, perform steps 8 through 17. Name the currently chosen trajectory the 'third segment'. The starting, second and third segment chosen in the simplified figures are shown in blue in Figure 4.5.4.
8. Check if the desired ending criteria are met. In the simplified figures, this would happen if the third segment passed through the end region. Note that this is the case. In the case of real situations, this would happen if the third segment is a stable asymptotic trajectory outside of the Hill-Sphere of the Earth-Moon system. If the criteria are met, the transfer is saved and the script returns to the next trajectory of step 7. Otherwise, the script continues with step 9.
9. Find all the trajectories that cross the path of the third segment after it has crossed the second segment.
10. For each of the trajectories found in step 9, perform steps 11 through 17. Name the currently chosen trajectory the 'fourth segment'.
11. Check if the desired ending criteria are met. This would happen if the fourth segment is a stable asymptotic trajectory outside of the Hill-Sphere of the Earth-Moon system. If the criteria are met,

the transfer is saved and the script returns to the next trajectory of step 10. Otherwise, the script continues with step 12.

12. Find all the trajectories that cross the path of the fourth segment after it has crossed the third segment.
13. For each of the trajectories found in step 12, perform steps 14 through 17. Name the currently chosen trajectory the 'fifth segment'.
14. Check if the desired ending criteria are met. This would happen if the fifth segment is a stable asymptotic trajectory outside of the Hill-Sphere of the Earth-Moon system. If the criteria are met, the transfer is saved and the script returns to the next trajectory of step 13. Otherwise, the script continues with step 15.
15. Find all the trajectories that cross the path of the fifth segment after it has crossed the fourth segment.
16. For each of the trajectories found in step 15, perform step 17. Name the currently chosen trajectory the 'sixth segment'.
17. Check if the desired ending criteria are met. This would happen if the sixth segment is a stable asymptotic trajectory outside of the Hill-Sphere of the Earth-Moon system. If the criteria are met, the transfer is saved and the script returns to step 2. Otherwise, the script returns to the next trajectory of step 16. No more than six segments are allowed, to limit the running time of the script.

This script results in a collection of transfers constructed with the limitless approach. Two things should be noted here. First of all, when using all the trajectories in the database, the limitless approach script running time became longer than the planning of this research allowed. Therefore, the choice was made to use only 25% of the database, chosen at random. Section 5.5 discusses the robustness of the script using this amount of trajectories. The second thing that should be noted is that, theoretically, the transfers found with the previous approaches should also be found through the limitless approach if the full dataset is used. However, since only a section of the database is used, it is entirely possible that the best transfers from other approaches are not found in the limitless approach.

5

Complete Low Energy Transfers: Results

This Chapter shows the results for each of the four transfer approaches, including the complete set of possible transfers, their required ΔV and transfer time, and explanations of phenomenon encountered in these results. Sections 5.1 through 5.4 take a look at the transfers per configuration. Additionally, the robustness of the results is discussed in Section 5.5. The results are compared in Chapter 6.

5.1. Standard approach

The set of 37 standard approach transfers found with a ΔV below 150 m/s is shown in Figure 5.1a. The starting points of each transfer are on the negative y-axis. From here, they follow non-transit trajectories which bring them to the vicinity of the Sun-Earth L_2 point, seen on the right side of the image.

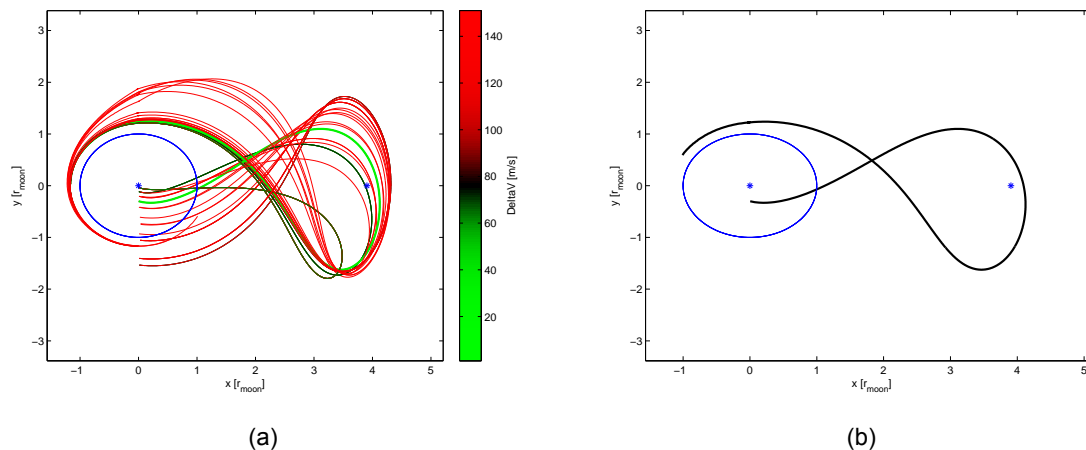


Figure 5.1: Standard approach transfers, shown in the CR3BP. The blue asterisk at the origin is the Earth, the blue circle around this is the orbit of the Moon. The blue asterisk on the positive x-axis is the Sun-Earth L_2 Lagrange point. The Sun is positioned on the negative x-axis. All other lines in the figure are standard approach transfers. Transfers start on the negative y-axis and end at the Earth-Moon L_2 Lagrange point. (a) shows each of the standard approach transfers with a ΔV below 150 m/s. The colours indicate the required amount of ΔV . (b) shows the standard approach transfer with the lowest ΔV . This transfer requires a ΔV of 28.2 m/s and a transfer time of 152.5 days.

Note that not all of the transfers travel all the way past the Lagrange point: Some non-transit trajectories start their return in the direction of the Earth before they reach this distance. This is expected for non-transit trajectories. Asymptotic trajectories would not show this behaviour. When the transfer return in the direction of Earth, they link into an asymptotic trajectory in the Earth-Moon system on the positive

y-axis. The figures clearly shows that some of these links require a change in direction, visible as a sudden curve in the transfer. This change in direction required ΔV , as can be seen from the fact that transfers with a larger change in direction are bright red in the image. After the link, the transfer follows the asymptotic trajectory in the Earth-Moon system until arrival at the Earth-Moon L_2 point. The location of this point upon arrival of the spacecraft is variable with the rotation of the Moon around the Earth.

Figure 5.1b shows the transfer with the least ΔV . The change in direction at the link on the positive y-axis is seen to be small, as expected for a transfer with low ΔV . This transfer requires a ΔV of 28.2 m/s, and has a transfer time of 152.5 days. The starting point of the transfer is at approximately 115,700 km from the centre of the Earth.

This optimal transfer, and the total set of transfers, is now compared to the transfer shown by Koon et al. (2001), in order to validate the found trajectories and transfers. The transfer described in the paper is a simplification of the transfer used by the Hiten mission. It uses a non-transit trajectory in the Sun-Earth system, which transfers to a trajectory which allows ballistic capture by the Moon. This second segment is different from the standard approach described here, since it does not end at the Earth-Moon L_2 point. However, lacking any other literature giving a detailed description of a low energy transfer to the Moon, the Hiten transfer is the best available option for validation.

The Hiten transfer has a ΔV of 34 m/s, in the same range as the optimal standard approach transfer found. A visual comparison of the two transfers shows that, although the first segment of the Hiten transfer is very similar to many of the standard approach transfers shown in Figure 5.1a, the second segment follows a different path. Thus, the standard approach works exactly as would be expected based on Koon et al. (2001): A very similar first segment with a different second segment, and with a ΔV in the same range.

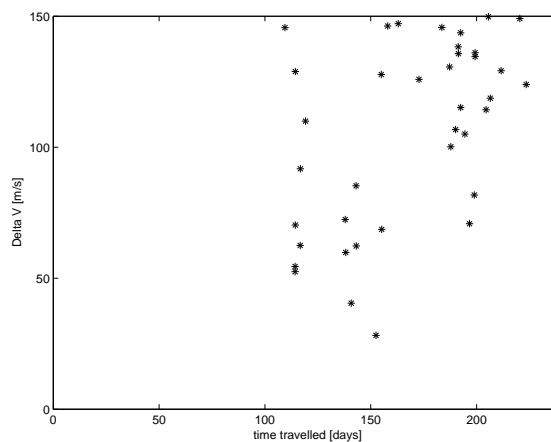


Figure 5.2: The transfer time and ΔV for the standard approach transfers. The transfer time starts where the transfer leaves the negative y-axis, and ends when it arrives at an elliptical orbit around the Earth-Moon L_2 Lagrange point.

Figure 5.2 shows the relationship between ΔV and transfer time for the standard approach. Note that the minimum transfer time for this type of transfers seems to be around 100 days. A lot of options for transfers near the minimum transfer time are possible, over a large range of ΔV . The lowest ΔV near the minimum transfer time is 52.5 m/s, at a transfer time of 114 days. To get the minimal ΔV an increase in transfer time is required.

To further understand the relationship between transfer time and ΔV , we compare the behaviour of transfers which are near the minimum of both these variables. Figure 5.3a shows the ten transfers with the lowest ΔV , and Figure 5.3b shows the ten transfers with the lowest transfer time. Figure 5.3a shows that there is some variety in low ΔV transfers. Both the first and the second segment show

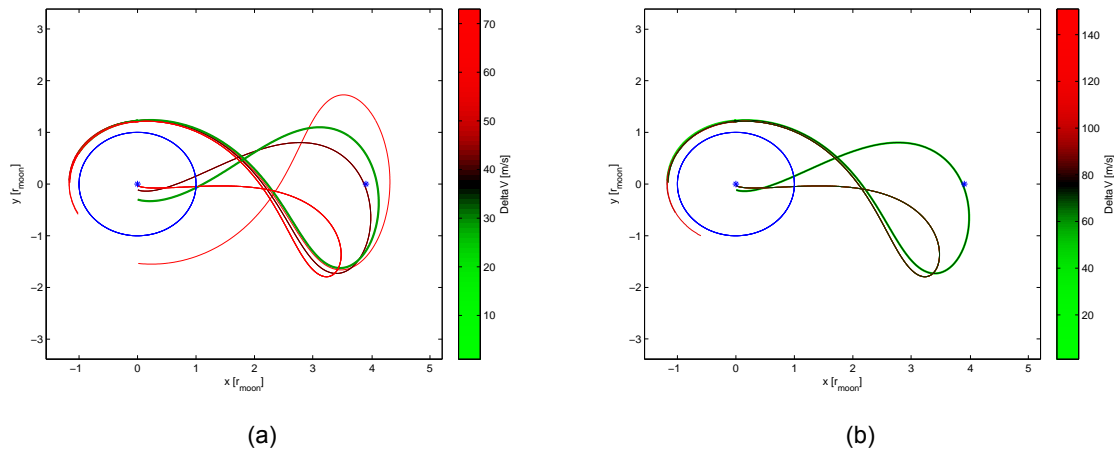


Figure 5.3: Standard approach transfers, shown in the CR3BP. The blue asterisk at the origin is the Earth, the blue circle around this is the orbit of the Moon. The blue asterisk on the positive x-axis is the Sun-Earth L_2 Lagrange point. The Sun is positioned on the negative x-axis. All other lines in the figure are standard approach transfers. Transfers start on the negative y-axis and end at the Earth-Moon L_2 Lagrange point. The colours indicate the required amount of ΔV . The transfer with the lowest ΔV has been made bold. (a) shows the ten standard approach transfers with the lowest ΔV . (b) shows the ten standard approach transfers with the lowest transfer time.

different options. In comparison, Figure 5.3b shows very little variety. The ten transfers all follow one out of two non-transit trajectories in the first segment, only deviating in the second segment. These two non-transit trajectories are both trajectories that stay relatively close to Earth when compared to the full set shown in Figure 5.1a. This explains the shorter transfer time. The transfers with low ΔV , in comparison, may take a longer non-transit trajectory, allowing their link to the second segment to be smoother.

When comparing Figures 5.2, 5.3a and 5.3b, some conclusions may be drawn. First of all, from the low variety in the first segment of transfers with low transfer time, it may be concluded that the difference between transfer times of the first segment trajectories is larger than the differences in transfer time of the second segment trajectories. This is expected, since the spatial differences of these trajectories are larger than the differences of trajectories in the second segment. Also, some transfers are in the best ten when concerning both ΔV and transfer time. However, a reduction of transfer time of some percentage will lead to an increase in ΔV of a far larger percentage.

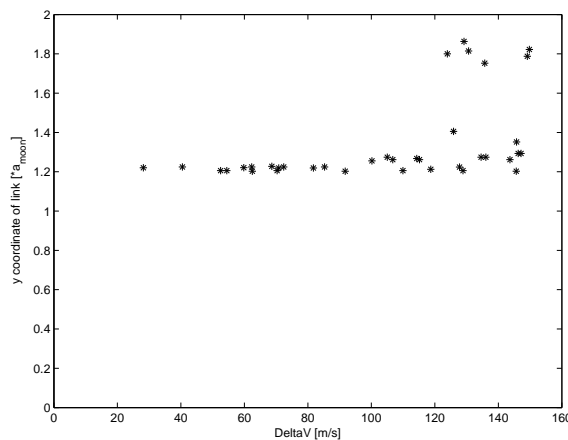


Figure 5.4: The ΔV and y-location of the link between segments for each of the standard approach transfers. The y-location is measured as a multiplication of the semi-major axis of the Moon's orbit.

The standard approach also allows for a simple visualization of the relation between the link location and the required ΔV for this link. Because the link between the segment is always on the positive y -axis, the y coordinate is the only variable in the location of the link. Figure 5.4 shows this relation. It is immediately noticed that no links were found at a distance of less than approximately 1.2 times the distance of the Moon from the Earth. This limit is caused by the limits set for the Hill spheres as were discussed in Chapter 3. The trajectories of the second segment do not come in the region closer to the Earth because of the Hill sphere of the Earth-Moon system. Since there are no second segment trajectories present in this region, there are no links possible.

It is further noticed that all the transfers with a relatively low ΔV are very near to this Hill sphere. This is supported by an inspection of the links on the positive y -axes in Figure 5.1a. The change in direction between the two segments is larger for transfers with a link on a high y -coordinate than for a link on a lower y -coordinate.

5.2. Three asymptotic segments

The set of 92 three asymptotic segment transfers found with a ΔV of less than 250 m/s is shown in Figure 5.5a. The starting point of each transfer is on the negative y -axis. From there, an asymptotic trajectory is followed toward an elliptic orbit around the Sun-Earth L_2 . From this ellipse, a link is made to an asymptotic trajectory back into the direction of the Earth. Note that the elliptic orbit itself is not shown, to prevent cluttering of the figure. The asymptotic trajectory in the direction of the Earth links with an asymptotic trajectory in the Earth-Moon system at the positive y -axis. Note that only two options are found for this link, which both clearly show a change in direction. This change in direction requires ΔV . This is also seen in the colour of the transfers: All found transfers are bright red, indicating high values for ΔV .

Figure 5.5b shows the transfer with the least total ΔV . This transfer requires a total ΔV of 184.0 m/s, and has a transfer time of 288.2 days. The starting point of this transfer is at approximately 266,000 km from the centre of the Earth.

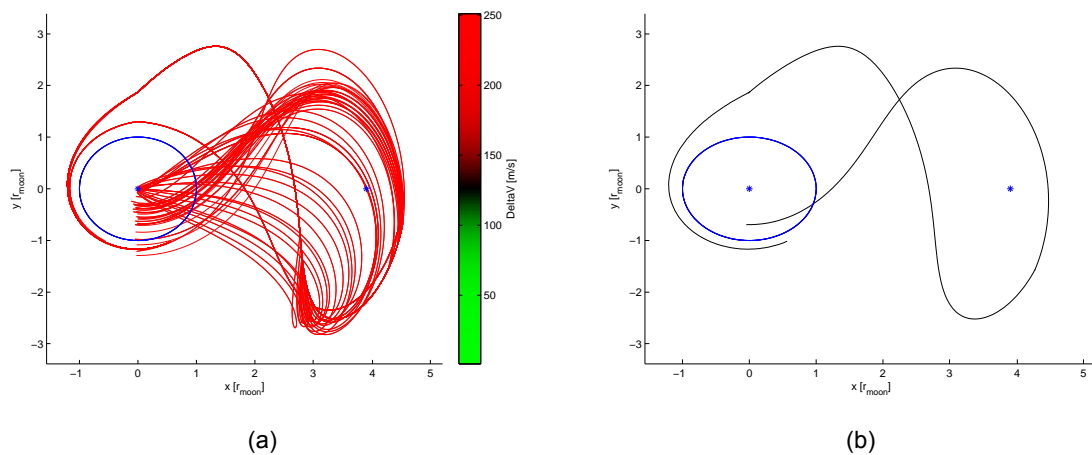


Figure 5.5: Three asymptotic segments approach transfers, shown in the CR3BP. The blue asterisk at the origin is the Earth, the blue circle around this is the orbit of the Moon. The blue asterisk on the positive x -axis is the Sun-Earth L_2 Lagrange point. The Sun is positioned on the negative x -axis. All other lines in the figure are three asymptotic segment approach transfers. Transfers start on the negative y -axis and end at the Earth-Moon L_2 Lagrange point. (a) shows each of the three asymptotic segments approach transfers with a ΔV below 250 m/s. The colours indicate the required amount of ΔV . (b) shows the three asymptotic segments approach transfer with the lowest ΔV . This transfer requires a ΔV of 184.0 m/s and a transfer time of 288.2 days.

Figure 5.6 shows the relationship between total ΔV and transfer time for the standard approach. When looking closely at this image, one can identify sets of points which together form a line with a somewhat negative slope. These lines are visible throughout the entire dataset, but most prominently at the top of

the image. Additionally, near the minimum transfer time a set of individual points is seen that do not follow the previously described lines. These phenomenon are not easily explained through only this figure.

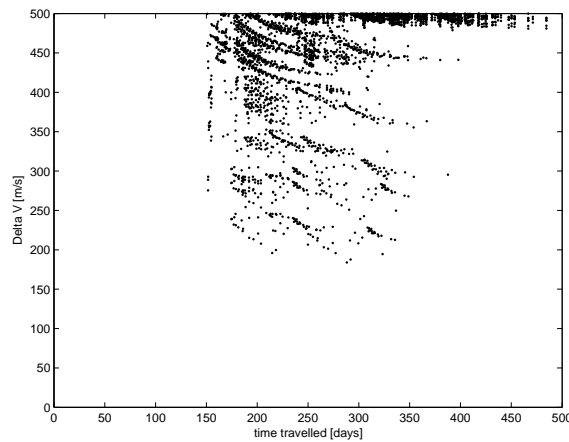


Figure 5.6: The transfer time and ΔV for each of the three asymptotic segments approach transfers. The transfer time starts where the transfer leaves the negative y-axis, and ends when it arrives at an elliptical orbit around the Earth-Moon L_2 Lagrange point.

To gain additional insights into the phenomenon observed, Figure 5.7a shows the ten transfers with the lowest ΔV , and Figure 5.7b shows the ten transfers with the lowest transfer time.

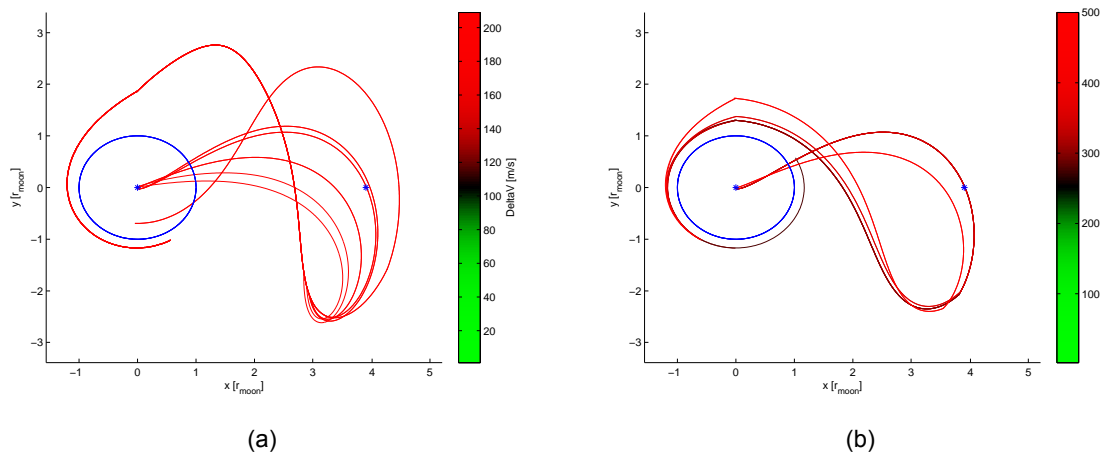


Figure 5.7: Three asymptotic segments approach transfers, shown in the CR3BP. The blue asterisk at the origin is the Earth, the blue circle around this is the orbit of the Moon. The blue asterisk on the positive x-axis is the Sun-Earth L_2 Lagrange point. The Sun is positioned on the negative x-axis. All other lines in the figure are three asymptotic segments approach transfers. Transfers start on the negative y-axis and end at the Earth-Moon L_2 Lagrange point. The colours indicate the required amount of ΔV . The transfer with the lowest ΔV has been made bold. (a) shows the ten three asymptotic segments approach transfers with the lowest ΔV . (b) shows the ten three asymptotic segments approach transfers with the lowest transfer time.

Figure 5.7a shows that all the transfers with lower ΔV use the same second and third segment. This suggests that the impact of the second link on the total ΔV is larger than the impact of the first link. This does not directly explain the behaviour seen in Figure 5.6.

Figure 5.7b shows that the variation of transfers with low transfer time is larger than seen for low ΔV . This seems to relate to the individual points with low transfer time seen in Figure 5.6. These transfers

stay close to the Earth in each of the three segments, compared to the other transfers seen in Figure 5.5a. This explains their low transfer times. Additionally, they use different links between the second and third segment. It is thus seen that the transfers which use the same second link follow the trend-lines in Figure 5.6, and those that use different links do not follow the trendlines.

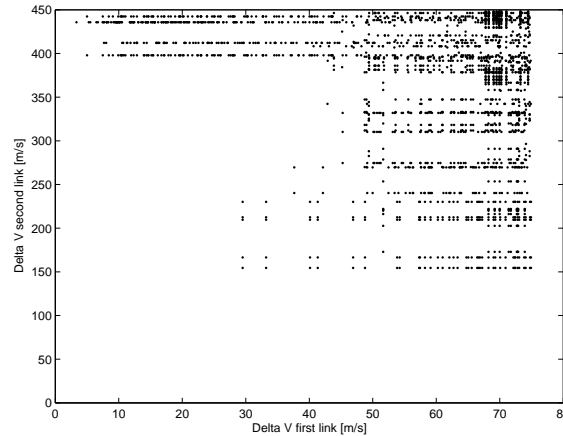


Figure 5.8: The relation between the first and the second burn of the three asymptotic segment approach transfers. The first burn is performed near the ellipse around the Sun-Earth L_2 Lagrange point. The second burn is performed on the Poincaré cut on the positive y-axis.

To further understand the trend-lines, Figure 5.8 shows the ΔV required for the first and second link of each transfer. It shows that the second burn has a far higher ΔV required than the first burn. This explains the trend-lines in Figure 5.6: Each of these curves belongs to a specific combination of second and third segments. This link determines most of the ΔV , and the link between the first and second segment contributes only little to the total ΔV . Additionally, it becomes apparent that when the second link uses less ΔV , the transfer time becomes higher, which causes the shape of the curves.

This difference in ΔV for the two different burns is explained by the layout of the transfers. The first burn takes place on the ellipse around the Sun-Earth L_2 Lagrange point, where trajectories run in almost exactly the same direction. There is no change in direction needed, only a small change in speed, which is done with a low ΔV requirement. The second burn, on the other hand, requires a significant change in direction, as can be seen in Figure 5.5a. It can be concluded that the layout of asymptotic segments is not a good fit to a link on the Poincaré cut on the positive y-axis. It is possible that links in other locations required less ΔV . If this is the case, it should be found in the limitless approach, which uses all trajectories and all locations of linking, thus including three asymptotic segment approach transfers with a free location of the second link.

5.3. Free location of linking

The set of 2140 transfers found with a ΔV of below 100 m/s is shown in Figure 5.9a. Again, the starting point of each transfer is on the negative y-axis. From there, non-transit trajectories are followed which approach the Sun-Earth L_2 point before returning in the direction of the Earth. There, they link up with asymptotic trajectories in the Earth-Moon system. Because the location of this link is not set, some interesting phenomena occur. First of all, it is noted that some transfers make an extra revolution around the Earth. In Figure 5.9a, these 'detour transfers' are visible as the set of curves moving about halfway between the Earth and the Moon. Some of these are shown in green and thus have a low ΔV . Apparently, following this extra curve in the transfer allows for a smooth linking to the second segment. The second phenomenon that is visible is what we will call 'shortcut transfers'. One of these is easy to see in Figure 5.9a. It starts as the second lowest on the negative y-axis, at almost twice the distant of the Moon to the Earth. From there, it immediately moves towards the Earth-Moon L_2 point, instead of

first following the non-transit trajectory. These shortcut transfers all start at a distance from the Earth that is larger than that of the Moon. As such, they are very ineffective, and are not considered viable options for this research.

Figure 5.9b shows the transfer with the least ΔV . This trajectory requires a ΔV of 8.8 m/s, and has a transfer time of 119.2 days. The starting point of this transfer is at approximately 589,600 km from the centre of the Earth.

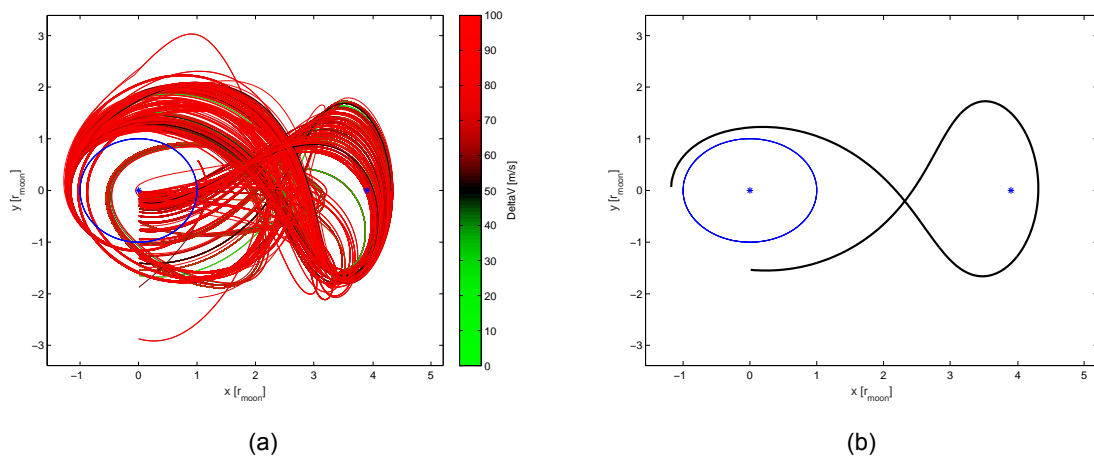


Figure 5.9: Free linking approach transfers, shown in the CR3BP. The blue asterisk at the origin is the Earth, the blue circle around this is the orbit of the Moon. The blue asterisk on the positive x-axis is the Sun-Earth L_2 Lagrange point. The Sun is positioned on the negative x-axis. All other lines in the figure are free linking approach transfers. Transfers start on the negative y-axis and end at the Earth-Moon L_2 Lagrange point. (a) shows each of the free linking approach transfers with a ΔV below 100 m/s. The colours indicate the required amount of ΔV . (b) shows the free linking approach transfer with the lowest ΔV . This transfer requires a ΔV of 8.8 m/s and a transfer time of 119.2 days.

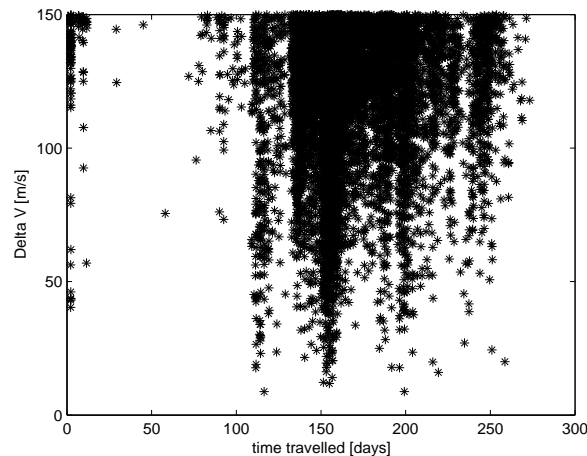


Figure 5.10: The transfer time and ΔV for the free linking approach transfers. The transfer time starts where the transfer leaves the negative y-axis, and ends when it arrives at an elliptical orbit around the Earth-Moon L_2 Lagrange point.

Figure 5.10 shows the relationship between ΔV and transfer time for the standard approach. The first thing we notice here are the shortcut transfers that were also seen in Figure 5.9a. All the transfers with a transfer time below 80 m/s are shortcut transfers. When looking at the rest of the set, it is noted that low ΔV and low transfer time are distinctly different sets, although no clear trends are immediately visible.

To understand why ΔV and transfer time do not match, we compare Figure 5.11a, which shows the ten

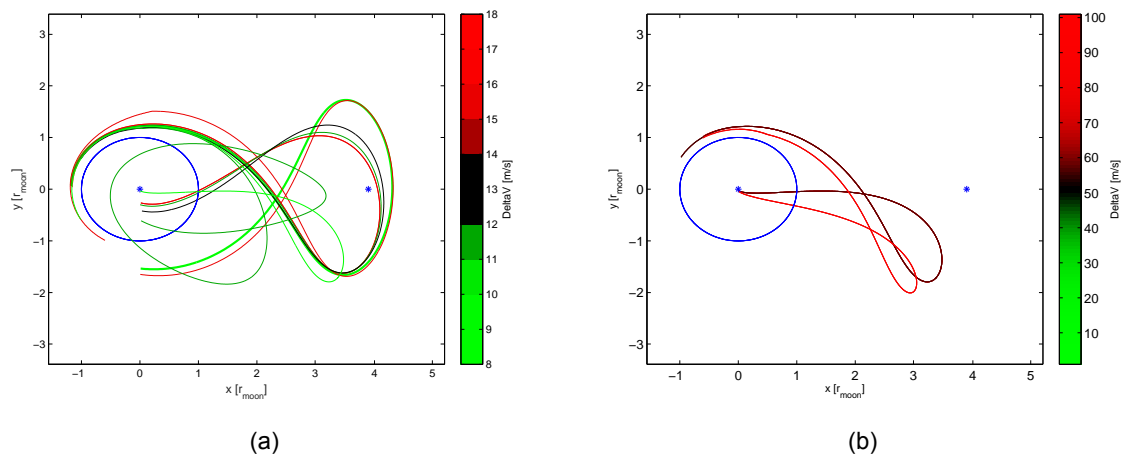


Figure 5.11: Free linking approach transfers, shown in the CR3BP. The blue asterisk at the origin is the Earth, the blue circle around this is the orbit of the Moon. The blue asterisk on the positive x-axis is the Sun-Earth L_2 Lagrange point. The Sun is positioned on the negative x-axis. All other lines in the figure are free linking approach transfers. Transfers start on the negative y-axis and end at the Earth-Moon L_2 Lagrange point. The colours indicate the required amount of ΔV . The transfer with the lowest ΔV has been made bold. (a) shows the ten free linking approach transfers with the lowest ΔV . (b) shows the ten free linking approach transfers with the lowest transfer time.

transfers with the lowest ΔV , and Figure 5.11b, which shows the ten transfers with the lowest transfer time (when not looking at shortcut transfers). From the comparison, it is immediately clear that the two sets follow very different paths. To get a short transfer time, a non-transit trajectory is chosen that does not fully reach the Sun-Earth L_2 point, similar to what was seen for standard approach transfers. For low ΔV the angle at which the two segments meet is most important, and it appears that less of a change in direction is needed for non-transit trajectories which do come very near to the elliptic orbit around L_2 . Additionally, a detour transfer is seen, which makes an extra revolution around the Earth. One thing that should be noted for the low ΔV transfers is their starting location: Some transfers have their starting point far beyond the distance of the Moon from the Earth. This is not a particularly effective way of transfer for the satellites. However, in the set of low ΔV transfers, several options starting near to the Earth are also available.

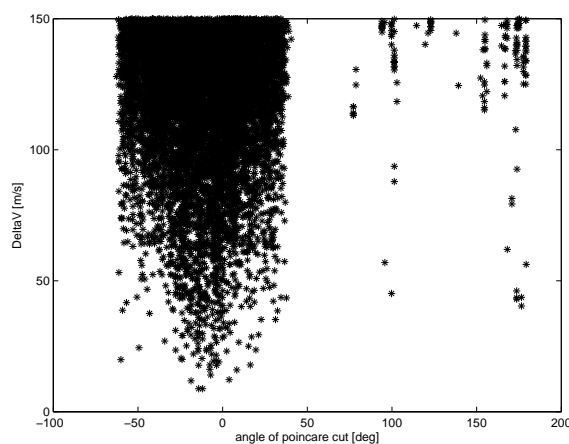


Figure 5.12: The angle of the link location and ΔV for each of the free linking approach transfers. The angle of the link is measured counter-clockwise with respect to the positive y-axis.

To take a look into the effect of freeing the location of the linking, Figure 5.12 shows the relationship be-

tween the location at which the transfer segments meet and the required ΔV . The location is described as an angle, where 0 degrees is the Poincaré cut on the y-axis as is used in the standard approach, and counter-clockwise rotation is positive. Note that shortcut transfers were removed in this figure. This figure shows two distinguishable groups of transfers. The left, main group are the 'normal' transfers. For this group it can be seen that there is an optimal angle for the link angle at 14 degrees clockwise from the y-axis. The second group, to the right of the image, is far more sparse. These are transfers of which the first, non-transit segment folds around the Earth, whereas other non-transit trajectories move away. Because the segment folds close to the Earth, they can meet up with the Earth-Moon segment at a far higher angle. Although this is interesting behaviour, it does not result in lower ΔV . Nonetheless, from the main group it is clear that the variation of the Poincaré cut is beneficial for ΔV , as was also seen for transfers in the Sun-Earth system (Langemeijer, 2018).

5.4. All classes, all link locations

The 119 limitless approach transfers found with a ΔV below 50 m/s is shown in Figure 5.13a. First of all, note that for this approach, the transfers do not start on the negative y-axis. Instead, they start at the negative x-coordinate equal to the distance between the Earth and the Moon. This change was used to allow some extra freedom in the links, allowing transfers between trajectories to happen somewhat earlier. The effect of this change is visible in the large loops around the Earth onto the positive y-axis. These loops exist of only one trajectory, so no links are used to make them. Secondly, in the lower segment of the figure, the same shortcut transfers as seen with the free linking approach are present. For the rest of the discussion, these transfers are ignored, since they are not useful for the research. Lastly, this figure shows a far greater variety in transfers than the previous approaches. This is exactly as expected; there are less restrictions and therefore more options become available.

Figure 5.13b shows the transfer with the least total ΔV when ignoring shortcut transfers. This transfer requires a total ΔV of 19.5 m/s, has a transfer time of 260 days, begins at 138,200 km from the centre of the Earth and has two segments. This transfer fits under the free linking approach transfers, since it begins with a non-transit trajectory in the Sun-Earth system and continues with an asymptotic trajectory in the Earth-Moon system.

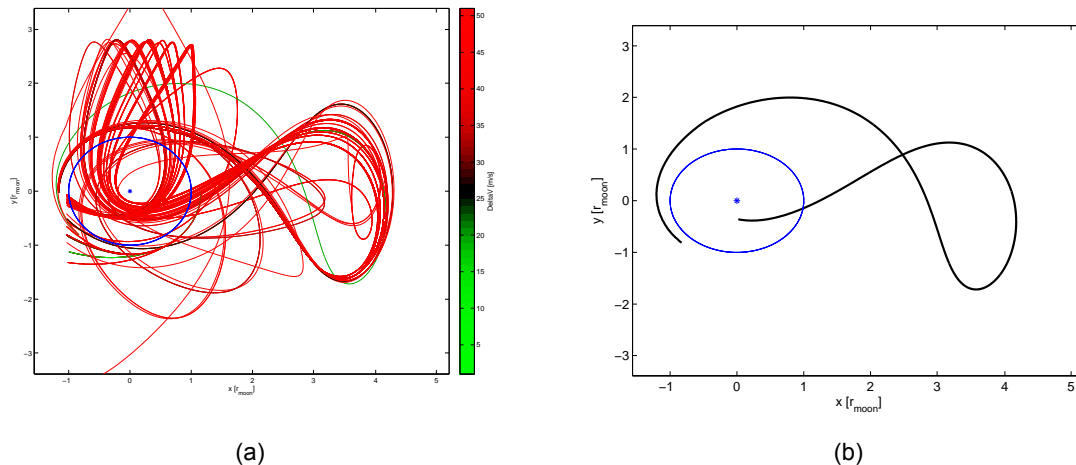


Figure 5.13: Limitless approach transfers, shown in the CR3BP. The blue asterisk at the origin is the Earth, the blue circle around this is the orbit of the Moon. The blue asterisk on the positive x-axis is the Sun-Earth L_2 Lagrange point. The Sun is positioned on the negative x-axis. All other lines in the figure are limitless approach transfers. Transfers start on the negative y-axis and end at the Earth-Moon L_2 Lagrange point. (a) shows each of the limitless approach transfers with a ΔV below 50 m/s. The colours indicate the required amount of ΔV . (b) shows the limitless approach transfer with the lowest ΔV . This transfer requires a ΔV of 19.5 m/s and a transfer time of 260 days.

Figure 5.14 shows the relationship between total ΔV and transfer time for the standard approach. Transfer times start at 200 days. Everything below this was removed, since they were all shortcut transfers.

The remaining data shows a trend towards a minimum at approximately 20 m/s and 260 days of transfer time. Obviously, the data are somewhat sparse, so the actual minimum may actually be located differently. It should be noticed here that transfer times are higher than for the free linking approach. This is caused by the additional loop followed at the beginning of the transfer. Therefore, it seems that the minimum of the limitless approach actually would match the minimum of the free linking approach if the full dataset were used.

The limitless approach allows for a great variety in transfers. To understand what kind of transfers work well for low ΔV and transfer time, we look at the top ten for each of these variables. Figure 5.15a shows the ten transfers with the lowest ΔV . Figure 5.15b shows the ten transfers with the lowest transfer time. The first thing that should be noticed is that all transfers shown here also fall under the category of free linking approach transfers, using only two segments. Secondly, we may note that there is more variety in the low ΔV transfers. This fits the spreading of data-points seen in Figure 5.14, where there is a dense clutter of low transfer time and more spread in the low ΔV range.

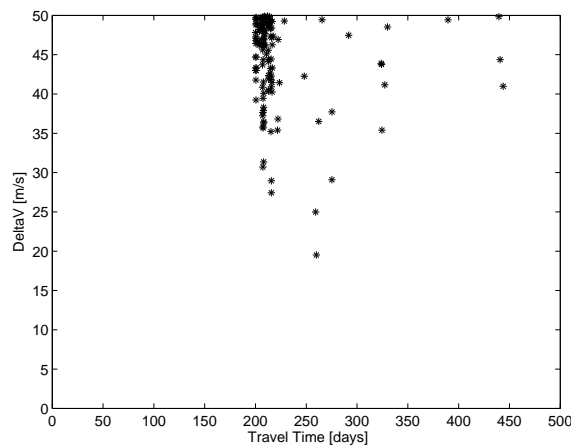


Figure 5.14: The transfer time and ΔV for each of the limitless approach transfers. The transfer time starts where the transfer leaves the negative y-axis, and ends when it arrives at an elliptical orbit around the Earth-Moon L_2 Lagrange point.

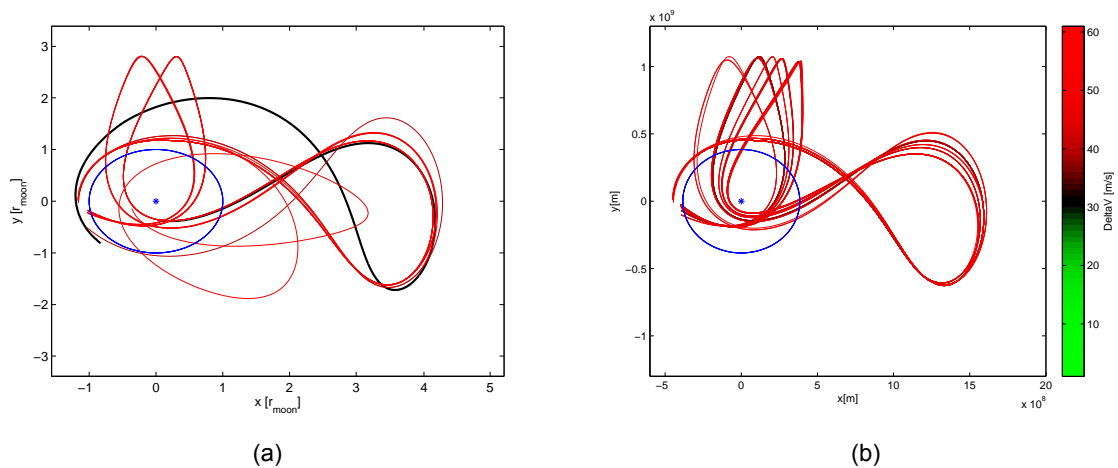


Figure 5.15: Limitless approach transfers, shown in the CR3BP. The blue asterisk at the origin is the Earth, the blue circle around this is the orbit of the Moon. The blue asterisk on the positive x-axis is the Sun-Earth L_2 Lagrange point. The Sun is positioned on the negative x-axis. All other lines in the figure are limitless approach transfers. Transfers start on the negative y-axis and end at the Earth-Moon L_2 Lagrange point. The colours indicate the required amount of ΔV . The transfer with the lowest ΔV has been made bold. (a) shows the ten limitless approach transfers with the lowest ΔV . (b) shows the ten limitless approach transfers with the lowest transfer time.

To see the effect of using more segments, we look at Figures 5.16a and 5.16b, which show the relationship between number of segments, ΔV and transfer time. It is immediately clear that an increased number of links does not create transfers with a lower ΔV or transfer time. It can be concluded that any one link which allows for making the transfer has a minimum ΔV that is so high, that any combination of two links always results in a ΔV above that of the optimum transfer. Also, it can be concluded that the use of additional transfers does not affect the total transfer time very much. There low transfer times seen with one link are shortcut transfers. When these are discarded, transfer times are similar for each number of links.

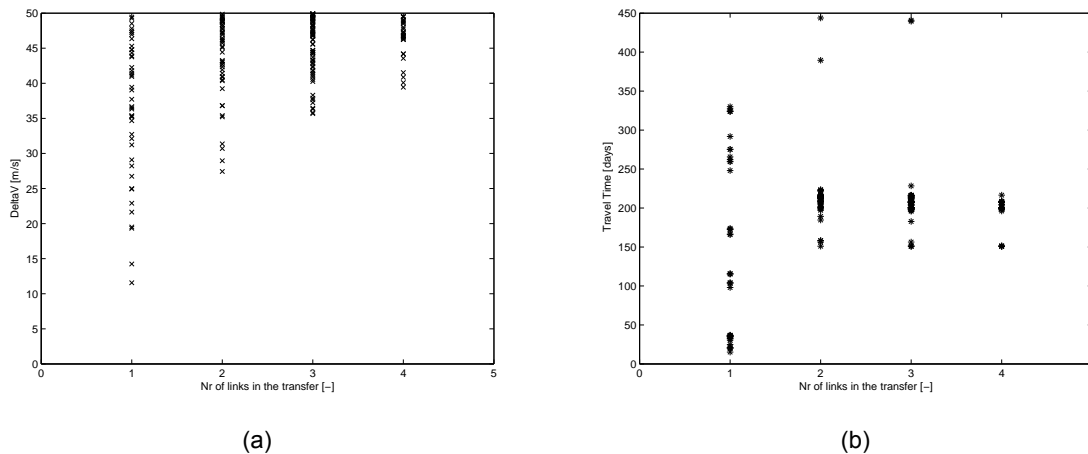


Figure 5.16: The relationship between number of links in a transfer and (a) the total ΔV or (b) the total transfer time required.

It should be noticed that the optimum transfer as was found for the free linking approach is not included in the result for the limitless approach, even though it should be possible to find this transfer using the limitless approach. This is caused by the fact that the limitless approach uses only 1/4th of the entire database, due to the required time to run the entirety of the script. Apparently, the trajectories which are needed to find the optimum of the free linking approach are not present in this subset. This also leads to the conclusion that the true optimum is not present in this set. Nonetheless, the trend shown in Figure 5.16a shows that it is highly unlikely that the limitless approach would result in a better optimum than the free linking approach.

Additional information that may be lifted from the results of the limitless approach is the behaviour of transfers with three asymptotic segments and free linking. Section 5.2 discussed that the three asymptotic segments approach was limited by the fixed location of linking. Since the limitless approach allows for all classes of trajectories and has free linking, there must be a subset in the result of three asymptotic segments with free linking. Because this subset behaves similarly to the normal free linking approach, it is only discussed briefly here.

The full set of transfers with three asymptotic segments from the limitless approach is shown in Figure 5.17a, and the transfer with the lowest ΔV is shown in Figure 5.17b. First of all, note that the limitless approach transfers were adapted slightly to start at the negative y-axis, like the three asymptotic segment approach transfers do, to have a fair comparison. Secondly, note that the main trends seen for three asymptotic segment transfers are still visible, with two sets of asymptotic trajectories in the Earth-Moon system. However, the sets are larger, and the links between the segments seem to be smoother.

This is supported by Figure 5.18, which shows the ΔV and transfer time. The lowest ΔV is found to be 27.4 m/s, with a transfer time of 216 days. This is significantly better than the optimum three asymptotic segment transfer with fixed linking location.

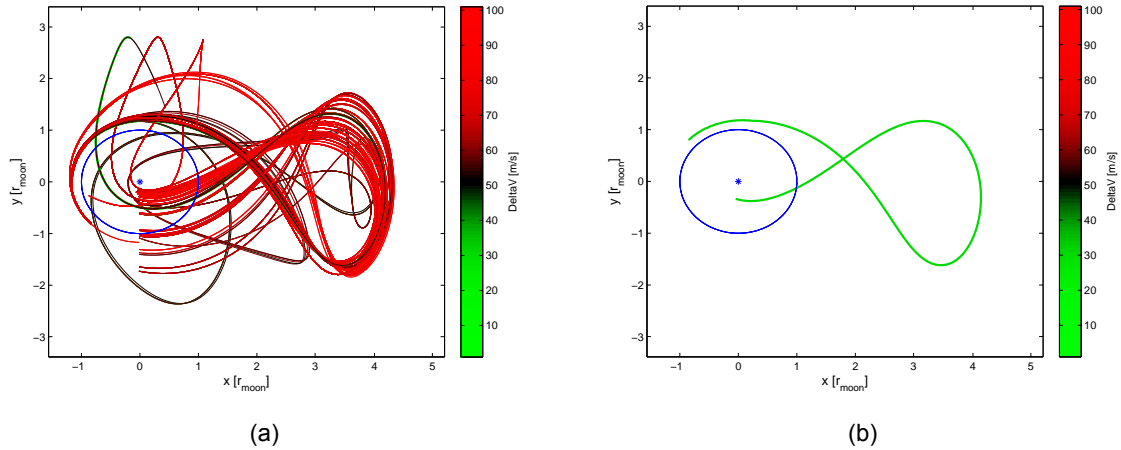


Figure 5.17: Three asymptotic segments with free linking approach transfers, shown in the CR3BP. The blue asterisk at the origin is the Earth, the blue circle around this is the orbit of the Moon. The blue asterisk on the positive x-axis is the Sun-Earth L_2 Lagrange point. The Sun is positioned on the negative x-axis. All other lines in the figure are limitless approach transfers. Transfers start on the negative y-axis and end at the Earth-Moon L_2 Lagrange point. (a) shows each of the three asymptotic segments with free linking approach transfers with a ΔV below 100 m/s. The colours indicate the required amount of ΔV . (b) shows the transfer with the lowest ΔV . This transfer requires a ΔV of 27.4 m/s and a transfer time of 216 days.

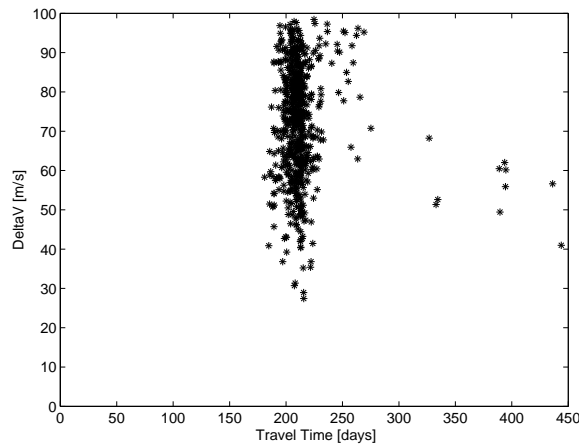


Figure 5.18: The transfer time and ΔV for each of the three asymptotic segments with free linking approach transfers. The transfer time starts where the transfer leaves the negative y-axis, and ends when it arrives at an elliptical orbit around the Earth-Moon L_2 Lagrange point.

It should be noted that these data were lifted from the full set of limitless approach transfers. For this approach, only a part of the database was used. It is therefore possible that a slightly better option exists within the full database. For comparison of the methods the available insights will have to suffice.

5.5. Robustness

All the results given above rely on the database that was created as discussed in Chapter 3. It is an important validation step to check the robustness of this database for the purpose of finding the optimum transfer. It is possible that the used database is too small, and that the use of a larger database would result in significantly better results.

In order to test the robustness of the database, each of the approaches were also considered when using subsets of the database. Runs using only 80%, 60% and 40% of the database, selected at random, were performed, so the results can be compared. Table 5.1 shows the results of this run. For each of the four approaches, the lowest ΔV found and the associated transfer time has been shown.

Table 5.1: Comparison of the found transfer with the lowest ΔV and the associated transfer time, when using only a specified percentage of the total database. The selection of trajectories is performed randomly.

	100%		80%		60%		40%	
	ΔV [m/s]	t [days]						
Standard	28.2	152.5	32.2	140.6	28.2	152.5	34.0	114.2
Three segments	184.0	288.2	187.6	288.4	184.0	288.2	323.7	308.7
Free linking	8.8	119.2	8.8	119.2	8.8	119.2	8.8	119.2
Limitless	19.5	260.0	19.5	260.0	25.0	259.0	25.0	259.0

From this table, it becomes clear that even when using smaller databases, the results stay mostly the same. Only for the three segment approach a sudden increase in minimum ΔV is seen when using 40% of the database. This can easily be explained by the removal of just a few trajectories from the dataset: Especially the second segment of the three segment approach is important to overall ΔV , as explained in Section 5.2. As the database gets smaller, those second segment trajectories that result in relatively low ΔV may be removed, resulting in a significant ΔV increase.

Overall, the database can thus be considered robust for the purpose of this study. There remains some risk at residing at a local optimum, but for the purpose of comparing different approaches this is allowable. Ongoing research into a transfer for a true mission might consider expanding the database, but need only do this for the optimum approach found in this research.

6

Comparing Low Energy Transfers: Discussion

This Chapter compares the results of the four approaches in areas important for transfer design, and discusses advantages and disadvantages of each of the approaches. Note that for the three asymptotic segments approach, the data for free linking from Section 5.4 are used. Section 6.1 discusses the ΔV and transfer time of each of the approaches. Section 6.2 discusses the options for scheduling the transfer for each of the approaches. Section 6.3 discusses the starting point of each of the approaches, being the location where a launcher vehicle should enter the spacecraft into the transfer trajectory. Based on these discussions, a complete comparison of the transfers and a list of their pros and cons are discussed in Section 6.4.

6.1. Comparison of ΔV and transfer time

Two elements to look at when choosing a transfer trajectory for any mission are the required ΔV and transfer time. This research concerns transfers for small satellites, which do not have access to a large engine or large amounts of fuel. Therefore, the required ΔV should be as low as possible. Transfer time is of secondary importance for the missions considered. However, in the case that ΔV is in the same range, transfer time can be a deciding factor.

Table 6.1 shows the ΔV and transfer time for two transfer trajectories per approach: Those of the transfer with the lowest ΔV and of the transfer with the lowest transfer time.

Table 6.1: The ΔV and transfer time for the lowest ΔV transfer and lowest transfer time transfer of each of the four approaches. Note that shortcut transfers found in the free linking and limitless approaches are not taken into account. Note that free linking is assumed for the three asymptotic segments approach.

	Lowest ΔV transfer		Lowest transfer time transfer	
	ΔV [m/s]	Transfer time [days]	ΔV [m/s]	Transfer time [days]
Standard	28.2	152.5	145.6	109.5
Three asymptotic segments	27.4	215.7	58.3	181.0
Free linking	8.8	119.2	126.9	71.9
Limitless	19.5	260.0	47.8	200.1

The first thing that may be noticed is that the three asymptotic segments approach and the standard approach use over twice as much ΔV as the free linking and limitless approach. The transfer time of the three asymptotic segments approach is also much higher. The free linking and limitless approaches score better on both accounts. From Chapter 5 we know that the ideal case for the limitless approach uses only one burn, and could therefore also be considered a free linking approach transfer. Apparently the free linking approach has the best behaviour for ΔV . This is caused by the angle at which the two segments of this transfer meet. An important aspect of the required ΔV is the change in direction that

is made at the link location. In the free linking approach, this change in direction is minimal, because of the lay-out of the trajectories used. Although the standard approach uses the same trajectories, the lay-out at the standard Poincaré cut is not optimal. The same was seen for the three asymptotic segments approach: The ΔV when using free linking was significantly lower than without free linking. However, the layout of the three asymptotic segments requires a larger change in direction, even when free linking is allowed. This leads to the conclusion that for both ΔV and transfer time, the free linking approach is the best option.

6.2. Comparison of scheduling

The scheduling options for the launch of a specific transfer are an important factor for mission planning. In the case of low energy transfers, scheduling is mostly limited by the position of the Moon upon arrival. With exception of the three asymptotic segments approach, none of the approaches have the option for a 'pause' in the transfer where the transfer may be synced with the Moon location, and therefore the moment of launch should be timed right. The three asymptotic segments approach allows for a syncing orbit around the Sun-Earth L_2 point, and is thus far less restricted in terms of scheduling. Especially for a mission with over a thousand satellites, this is essential.

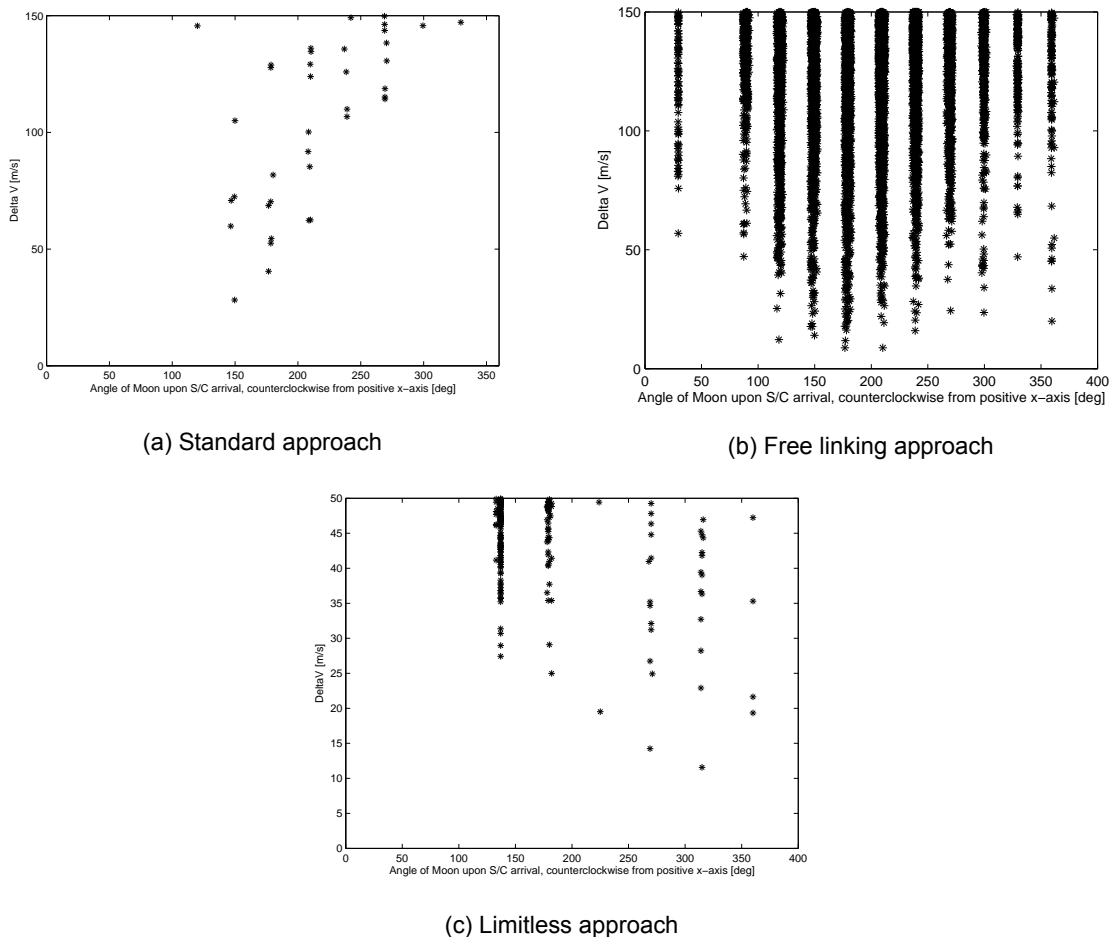


Figure 6.1: The angle of the Moon upon arrival and ΔV for each of the standard approach transfers. The angle of the Moon is measured counter-clockwise with respect to the positive x-axis.

Figures 6.1a, 6.1b and 6.1c show the relationship between the required ΔV of a transfer, and the location of the Moon upon arrival. The angle of the Moon is measured counter-clockwise with respect to the positive x-axis. In other words, an angle of arrival of 0 degrees means the Moon is exactly between the

Earth and the Sun-Earth L_2 point, whereas an angle of 180 degrees means the Moon is in between the Sun and the Earth. Because this research only included a limited number of possible Moon locations to limit the running time of the script, each of the figures shows data-points only on specific vertical lines. Despite these limited lines, the trends seem clearly visible, and unclarity is caused more by data sparsity than limited Moon locations.

Each of the approaches in Figure 6.1 shows a trend towards a minimum ΔV at specific angles of arrival, with increasing ΔV as the Moon moves away from that angle. The standard approach shows a minimum in the vicinity of 150 degrees. The free linking approach shows a minimum in the vicinity of 180 degrees. Interestingly, the free linking and limitless approach also show low values at very high angles. These are the data-points associated with the shortcut transfers discussed in Chapter 5. When removing these results, the limitless approach also shows a minimum around the 150 degree mark, which are the one-burn only transfers that were found, and which can also be described as free linking approach transfers.

It is interesting to study the situation around the optimum for each of the three approaches. The amount of increase in ΔV per deviation from the optimum arrival angle tells us how important it is to have proper scheduling. Although the sparsity of data in both the standard and the limitless approach makes it complicated to draw certain conclusions, an attempt is made. It can be seen in the figures that the free linking approach has the smallest sensitivity to a change in the angle of the Moon upon arrival. Nonetheless, if the Moon moves 90 degrees, ΔV is doubled. The standard approach shows far more sensitivity when the Moon Angle decreases than when it increases. This is fortunate, since a delay in launch will result in an increased angle of arrival. The limitless approach shows different behaviour around the optimum: There seems to be a somewhat flat base and after this, a sudden increase, when the shortcut transfers are not taken into account. The flat base may show similar behaviour to the free linking approach if more data-points are available, which would fit with the conclusion that limitless approach transfer with low ΔV are actually free linking approach transfers.

When comparing the different transfer approaches on the subject of scheduling, we may then conclude two things. First of all, the three segment approach is very beneficial for scheduling, since it allows for a syncing orbit around the Sun-Earth L_2 point, which makes it possible to use any launch moment. It should be noted that this significantly increases the transfer time: It will take almost one full month before the moon has returned to the desired location. Of the remaining approaches, sparsity of data makes definite conclusions impossible, but the free linking approach seems to show the most beneficial behaviour for scheduling. The limitless approach may show the same behaviour, but more research is required here to be certain.

6.3. Comparison of transfer starting point

Although this research is only concerned with the transfer itself in terms of ΔV and transfer time, the starting location of the transfer should be taken into account for the comparison. The research considers a transfer for small satellites, which are not capable of bringing themselves to the starting point of the transfer due to fuel constraints. However, the launcher should be capable of bringing one or multiple satellites into the transfer, and as such it is beneficial for the mission of the starting point of the transfer is in the vicinity of the Earth.

For ease of reference, the figures with the top ten transfers in terms of ΔV for each of the approaches have been repeated in Figures 6.2a through 6.2d. First of all, notice that both the standard approach and the free linking approach offer options that start at 11,790 km from the centre of the Earth, making use of the same non-transit trajectory. This is the starting point closest to the Earth from the low ΔV transfers. The free linking approach transfer with this starting point uses 8.8 m/s; the difference with the transfer with the lowest ΔV being only 0.01 m/s. In terms of starting point, this is clearly the optimal transfer.

When looking at the three asymptotic segments with free linking approach, the closest starting point lies at 69,030 km from the centre of the Earth, with a ΔV of 42.3 m/s. The limitless approach has the

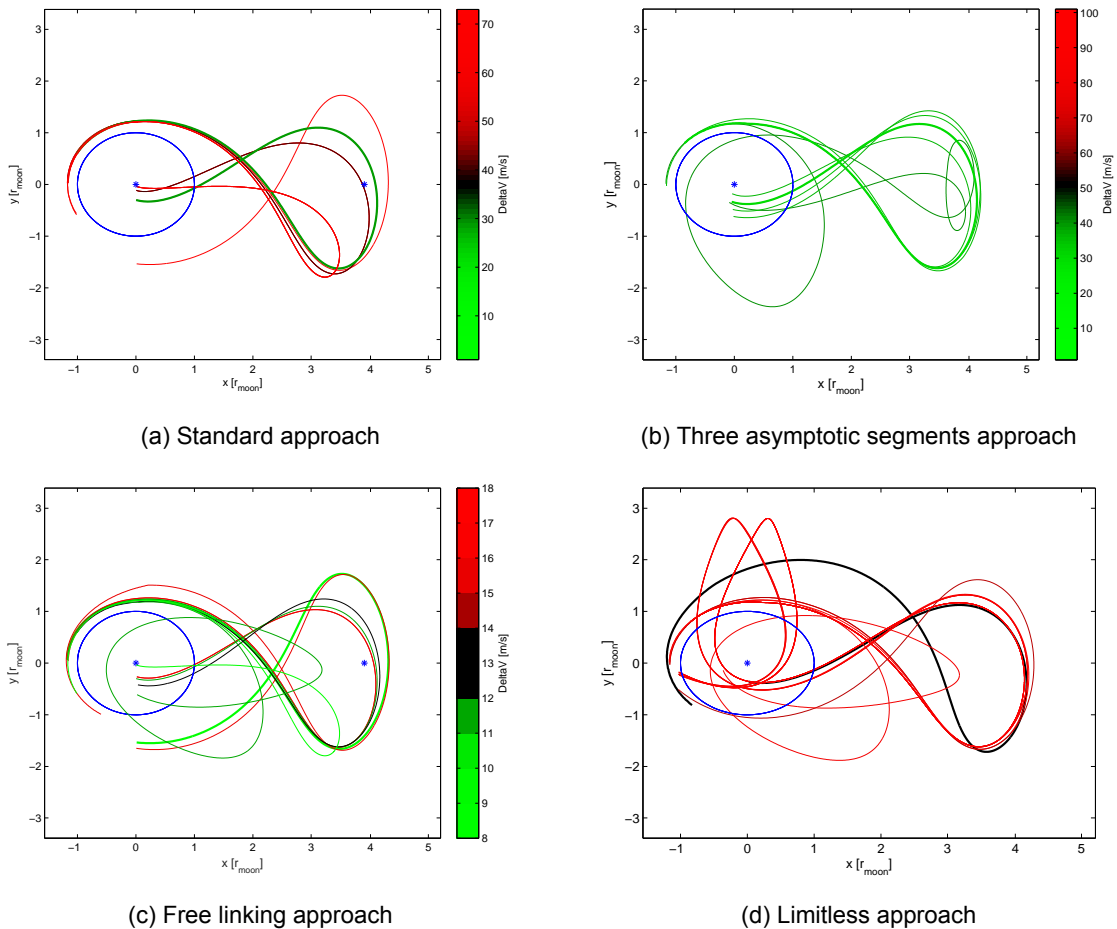


Figure 6.2: The ten transfers with the lowest ΔV of each of the approach transfers, shown in the CR3BP. The blue asterisk at the origin is the Earth, the blue circle around this is the orbit of the Moon. The blue asterisk on the positive x-axis is the Sun-Earth L_2 Lagrange point. The Sun is positioned on the negative x-axis. All other lines in the figure are the transfers. Transfers start on the negative y-axis and end at the Earth-Moon L_2 Lagrange point. The colours indicate the required amount of ΔV . The transfer with the lowest ΔV has been made bold.

closest starting point at 138,200 km from the centre of the Earth, with a ΔV of 19.5 m/s, which is the lowest ΔV transfer for this approach. These options are both considerably further away from the Earth than the option found for the free linking approach. This will increase the demands on the launcher vehicle significantly. It can thus be concluded that the free linking approach is optimal where transfer starting point is considered.

6.4. Complete comparison

Based on the topics discussed above we can look into each of the approaches and consider their applications, pros and cons.

6.4.1. Standard approach

The standard approach is the approach that is most like the research available about low energy transfers for lunar missions. It is described by (Koon et al., 2001) as a simplified version of the Hiten mission Uesugi et al. (1991) and follows similar layouts as described by (Koon et al., 1999), although for different planetary bodies.

This research has shown that the standard approach is not ideal in any situation. In any of the aspects considered, the free linking approach performs better. For mission applications, the standard approach is therefore discarded. However, the standard approach does have significant uses for validation, and

in a theoretical setting. It is the only approach for which previous research is available, making it invaluable for validating a database of low energy trajectories. Additionally, computation times for the standard approach are significantly lower than for any of the other approaches. As such, it can be valuable for making first estimations on ΔV and transfer time, before a more detailed study is done which allows a free location of linking.

6.4.2. Three segments approach

The three segments approach changes the standard approach to allow for a station-keeping orbit around the Sun-Earth L_2 point. It could be seen as an intermediate form between the Hiten and Genesis transfer trajectories Uesugi et al. (1991), Burnett et al. (2003), since the Hiten mission uses a transfer to the Moon, whereas the Genesis goes to the Sun-Earth L_1 and L_2 .

This research has shown that the three segment approach, when using a free location of linking, has similar ΔV requirements as the standard approach, although transfer times are longer and the starting point of the transfer is further from the Earth. The advantage of this approach is the option of a station-keeping orbit around the Sun-Earth L_2 point. Not only does this reduce the effect of a launch delay, it also allows for additional mission objectives in this L_2 orbit.

The three segments approach is most useful for missions with somewhat larger satellites, allowing for higher ΔV budgets and additional mission objectives at the Sun-Earth L_2 . Additionally, if a lunar mission considers the flexibility in scheduling more important than the initial ΔV required for the launcher rocket, it might be the best option for small satellite mission to the Earth-Moon L_2 . This would be very dependent on the mission: Missions which require a high number of satellites might consider scheduling more important than missions that require only few.

6.4.3. Free linking approach

The free linking approach allows for a free location of linking between the two segments of the standard approach. This additional freedom was researched by (Langemeijer, 2018) for a transfer between the Sun-Earth L_1 and L_2 , where it was found to be advantageous in ΔV . This research now proves that the same goes for a transfer to the Earth-Moon L_2 . ΔV reductions of over 60% are possible by freeing the location of the link.

Where ΔV and transfer time are concerned, the free linking approach clearly shows the best results of the four approaches. Additionally, the transfer starts closest to the Earth of the four approaches. However, where scheduling is concerned, the free linking approach is far more sensitive than the three segments approach. While small delays do not impact the ΔV very much, a delay of a week could potentially double the required ΔV .

The free linking approach is most useful for missions with a very tight ΔV budget or limited time frames for the transfer. The approach allows for a quick and 'cheap' transfer to the Earth-Moon L_2 point. However, for missions that require flexibility in scheduling, the free linking approach is not optimal. If a mission considers flexibility in planning of lesser importance than ΔV and/or transfer time, the free linking approach is the best option.

6.4.4. Limitless approach

The limitless approach was based on the suggestion by (Parker, 2007) that it might be possible to reduce the ΔV of a transfer by using multiple segments. It is an entirely novel research, and there is no available work for comparison.

The research has shown that the limitless approach does not improve upon the previous approaches. Adding additional segments to the transfer increases both ΔV and transfer time. In terms of ΔV reduction it converges to the free linking approach, and it shows very similar behaviour to this approach for scheduling and transfer starting point. As such, there are no situations in which it is better to plan for using a limitless approach over a free linking approach.

The advantage of the limitless approach is found in calculating the effects of deviations from a planned

transfer. It may be used to anticipate the optimal location of an extra burn when a previous one did not go entirely as planned, and to determine the amounts of extra fuel to bring for such situations.



Conclusions and Recommendations

This research intended to compare several options for combining low energy trajectories into transfers from the Earth to the Earth-Moon L_2 Lagrange point, aiming for low ΔV to allow small satellites to fly missions to this location. This Chapter discusses the best options for such missions, reflects on the methods used to get to these conclusions and does some recommendations for future work.

7.1. Conclusions of the research

Four configurations were created for this research, and their ΔV , transfer time, scheduling and transfer starting points were compared. It should be noted that of these factors, ΔV is the most important, because the effort of this research is to find a transfer which may be used by small satellites with very strict fuel constraints.

The free linking approach, using a non-transit trajectory in the Sun-Earth system and a stable asymptotic trajectory in the Earth-Moon system, with a free location of linking, is the optimal configuration for a low energy transfer for a mission from an Earth-orbit to a lunar L_2 orbit on tight ΔV constraints. ΔV requirements of below 15 m/s are possible while starting very close to the Earth, small delays of launch do not cause significant increases in ΔV , and the transfer time is relatively short for low energy transfers.

When a similar mission is considered with slightly less tight ΔV constraints, where either freedom in scheduling is considered more important than ΔV , or additional mission objectives at the Sun-Earth L_2 are considered, the three asymptotic segments approach with free linking is the best option. This approach allows for a station-keeping orbit around the Sun-Earth L_2 point at the cost of increasing ΔV to approximately 30 m/s, and moving the starting point of the transfer further away from the Earth.

Overall, it can be concluded that the standard approach which is used throughout literature can be improved upon to gain transfers which are of more use to missions going to the Earth-Moon L_2 point. Future missions intending to send small satellites towards this point, such as OLFAR, could make use of the methods described in this research to create their own transfer, bringing new discoveries about the origins of our universe another step closer.

7.2. Reflection on the methods

At the end of the research, some conclusions may be drawn about the methods used. Some choices turned out to not be ideal, whereas other decisions seem to have worked out quite well.

To get to the results of this research, a very linear approach was used. Initially, the full database of low energy trajectories was created. Only when this was done, the linking scripts were created to get to the full transfers. The advantage of this method is that the work-packages are very clear, and that no two parts of the work are happening at the same time. This is a great advantage in both planning and in effective working.

The downside of the linear approach is that it does not allow for much changes in previously finished steps. The research showed that specific classes of trajectories get used more often than others. For example, even in the limitless approach, transit trajectories are not used. Additionally, the trajectories with higher energy levels do not get used. This means that a significant portion of the database is useless. On the other hand, there is a sparsity of data at some points. As such, it might have been better to create a smaller initial database, and expand it after a initial linking is performed. This way, the database can get expanded only in those areas where it is used. The same goes for the angles of the Moon upon arrival. An initial run of the linking script with smaller database may have shown where the optimum conditions for the location of the Moon are, allowing the final run to focus on this area.

7.3. Recommendations for future work

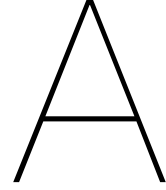
Due to time constraints, this research was limited in many areas. For future research with more available time, the following adaptations are recommendable:

- Use the full database in the limitless approach. In this research, only 25% of the trajectories were used. This could prove with certainty that the limitless approach converges to the free linking approach.
- Expand the database with trajectories similar to those that provide optimal transfers. This would include non-transit trajectories in the Sun-Earth system and stable asymptotic trajectories in the Earth-Moon system.
- Use a smaller interval between the possible angles of the Moon upon arrival, possibly only using a specific interval. From the results it is clear that there is an optimum location of the Moon. Additional research into more angles around this optimum could result in a further decrease of ΔV requirements.
- Set a restriction on the starting location of transfers. This restriction should be a specified distance from the Earth, likely somewhere within the orbit of the Moon. Transfers that do not fit within this restriction are not feasible for missions. This restriction will also prevent the shortcut transfers that were found for the free linking and limitless approach.
- Improve the script for finding the Lagrange Points. The current script uses manual adjustments, which should be automated.

Additionally, from this research follow some recommendations for future research:

- Additional research into the free linking and three asymptotic segments with free linking approaches in a three dimensional, non-circular four body system. This research only looks into two coupled planar CR3BP's. When taking the ellipticity and inclination of the orbits of the main bodies and the attraction of a third body into account, the results are bound to change. This report showed that the free linking approach is the most interesting for small satellite missions. Additional research is required if such a mission is to truly use such transfers.
- Additional research into the three asymptotic segments approach for dual-objective missions. This research focussed on small satellite missions with only an objective in orbit around the Earth-Moon L_2 point. However, additional scientific goals may be achieved by using a single satellite for a mission in orbit around the Sun-Earth L_2 which later moves on to the Earth-Moon L_2 . Because the fuel demands would be higher, this would have to be a larger satellite. More research into this area might prove or disprove the feasibility of such a mission.
- Investigate low thrust options. The current research assumes high-thrust burns at the linking locations. For small satellites low thrust options might be interesting. It might be possible to use the same combination of trajectories, or possibly other trajectory combinations become more interesting when using low thrust methods.

These conclusions and recommendations finalize the research on combinations of low energy trajectories for a Lunar L_2 mission.



Appendix: Trajectory creation script details

This appendix gives an overview of the code, settings, constants and other parameters used in the low energy trajectory creation script in TUDAT. Note that the full script can be found through Github (<https://github.com/AMPronk/Thesis>). To begin with, the constants which are used throughout the entire script are discussed in Section A.1. The script is covered in parts: Section A.2 covers the creation of the ephemeris model, which includes the Sun, Earth, Moon, spacecraft and L_2 points. Section A.3 the calculation of the sets of initial conditions, and Section A.4 the propagation of the trajectories.

A.1. Constants

The trajectory creation script makes use of a set of constants as the basis for all other variables. These constants are found in Table A.1, including their origins.

Table A.1: Constants used

Variable	Symbol	Value	Origin
Gravitational Parameter of the Sun	μ_{sun}	$1.32712440018E20 \text{ m}^3\text{s}^{-2}$	TUDAT value
Gravitational Parameter of the Earth	μ_{earth}	$3.986004418E14 \text{ m}^3\text{s}^{-2}$	TUDAT value
Gravitational Parameter of the Moon	μ_{moon}	4.9048695E12	TUDAT value
Orbital period of the Earth (sidereal year)	T_{earth}	31558149.504 sec	TUDAT value
Sidereal day	t_{day}	86164.091 sec	TUDAT value
Orbital period of the Moon	T_{moon}	27.322 sidereal days	Wertz et al. (2011)
Astronomical Unit	AU	149597873474.74 m	Eq. A.1
Moon orbit radius	r_{moon}	384051120.54 m	Eq. A.2

The distances between the main bodies are calculated using the re-ordered versions of equation 2.31:

$$AU = \sqrt[3]{(\mu_{sun} + \mu_{earth}) \frac{T_{earth}}{2\pi}} \quad (\text{A.1})$$

$$r_{moon} = \sqrt[3]{(\mu_{earth} + \mu_{moon}) \frac{T_{moon}}{2\pi}} \quad (\text{A.2})$$

A.2. Ephemeris Creation

The ephemeris creation script begins with creating the three main bodies: Sun, Earth and Moon. Each body is given the correct gravitational parameter, as found in Section A.1, and the initial conditions shown in table A.2.

Table A.2: Constants used

	Sun	Earth	Moon
semi-major axis	0	1 AU	$1 r_{moon}$
eccentricity	0	0	0
inclination	0	0	0
argument of periapsis	0	0	0
longitude of ascending node	0	0	0
true anomaly	0	0	0

Note that the Sun and the Earth both have the solar system barycentre as the point of origin, whereas the Moon uses the Earth as the point of origin as reference for the initial conditions. For these three bodies, the trajectories are not propagated. Instead, constant Keplerian trajectories are calculated by TUDAT.

Besides the three main bodies, a massless spacecraft is created in the ephemeris model. Depending on the class of trajectory that the ephemeris is used for, this spacecraft is either attracted by the Sun and the Earth, or the Earth and the Moon. At this point, the spacecraft does not yet have a position in the ephemeris model, since this will be added later.

The last thing to be added to the ephemeris model are the locations of the Lagrange points. They are implemented as massless spacecraft with initial conditions in the ephemeris model, attracted either by the Sun and the Earth, or the Earth and the Moon. When the initial condition has been set correctly, these spacecraft remain in the same relative position to their two main bodies. As explained in Section 2.3, the TUDAT script for finding Lagrange point turned out to have some rounding errors. Therefore, manual adjustments were performed to both the initial location and velocity. In the Sun-Earth system, the location of the Lagrange point was moved away from the Earth by 507.776127 meters, and the velocity in the rotating system was decreased by $4.48950212 \cdot 10^{-4}$ m/s. In the Earth-Moon system, the location of the Lagrange point was moved away from the Moon by 99,971.83293 meters, and the velocity in the rotating system was decreased by 0.95575 m/s.

A.3. Initial Conditions Calculation

Initial conditions for the spacecraft are created using equation 3.22. The values of α_1 , α_2 , β and t were varied to get different initial conditions. The sample size for each was found through trial and error, to get as much possible results within the allotted time. The minimum and maximum value were set in such a way that the entire range of allowed energy levels was covered, as was described in Section 3.5. Tables A.3 through A.8 show the used variables for the Sun Earth system, and tables A.9 through A.14 for the Earth Moon system

Table A.3: Used variables for stable asymptotic trajectories in the Sun-Earth system

	lowest value	highest value	sample size
α_1	0.0	0.0	1
α_2	-5.0E-2	5.0E-2	17
β	-5.0E-2	5.0E-2	68
t	0.0	3.0	17

Table A.4: Used variables for unstable asymptotic trajectories in the Sun-Earth system

	lowest value	highest value	sample size
α_1	-5.0E-2	5.0E-2	17
α_2	0.0	0.0	1
β	-5.0E-2	5.0E-2	68
t	0.0	3.0	17

Table A.5: Used variables for non-transit trajectories inside the Hill-sphere of the Sun-Earth system

	lowest value	highest value	sample size
α_1	-5.0E-2	0.0	17
α_2	-5.0E-2	0.0	17
β	-5.0E-2	5.0E-2	68
t	0.0	3.0	17

Table A.6: Used variables for non-transit trajectories outside the Hill-sphere of the Sun-Earth system

	lowest value	highest value	sample size
α_1	0.0	5.0E-2	17
α_2	0.0	5.0E-2	17
β	-5.0E-2	5.0E-2	68
t	0.0	3.0	17

Table A.7: Used variables for transit trajectories into the Hill-sphere of the Sun-Earth system

	lowest value	highest value	sample size
α_1	-5.0E-2	0.0	17
α_2	0.0	5.0E-2	17
β	-5.0E-2	5.0E-2	68
t	0.0	3.0	17

Table A.8: Used variables for transit trajectories out of the Hill-sphere of the Sun-Earth system

	lowest value	highest value	sample size
α_1	0.0	5.0E-2	17
α_2	-5.0E-2	0.0	17
β	-5.0E-2	5.0E-2	68
t	0.0	3.0	17

Table A.9: Used variables for stable asymptotic trajectories in the Earth-Moon system

	lowest value	highest value	sample size
α_1	0.0	0.0	1
α_2	-1.0E-2	1.0E-2	17
β	-1.0E-2	1.0E-2	68
t	0.0	3.0	17

Table A.10: Used variables for unstable asymptotic trajectories in the Earth-Moon system

	lowest value	highest value	sample size
α_1	-1.0E-2	1.0E-2	17
α_2	0.0	0.0	1
β	-1.0E-2	1.0E-2	68
t	0.0	3.0	17

Table A.11: Used variables for non-transit trajectories inside the Hill-sphere of the Earth-Moon system

	lowest value	highest value	sample size
α_1	-1.0E-2	0.0	17
α_2	-1.0E-2	0.0	17
β	-1.0E-2	1.0E-2	68
t	0.0	3.0	17

Based on these variables, sets of initial coordinates and velocities in the rotating system of the CR3BP can be calculated using equation 3.22. From these initial conditions, the energy level is calculated. If

Table A.12: Used variables for non-transit trajectories outside the Hill-sphere of the Earth-Moon system

	lowest value	highest value	sample size
α_1	0.0	1.0E-2	17
α_2	0.0	1.0E-2	17
β	-1.0E-2	1.0E-2	68
t	0.0	3.0	17

Table A.13: Used variables for transit trajectories into the Hill-sphere of the Earth-Moon system

	lowest value	highest value	sample size
α_1	-1.0E-2	0.0	17
α_2	0.0	1.0E-2	17
β	-1.0E-2	1.0E-2	68
t	0.0	3.0	17

Table A.14: Used variables for transit trajectories out of the Hill-sphere of the Earth-Moon system

	lowest value	highest value	sample size
α_1	0.0	1.0E-2	17
α_2	-1.0E-2	0.0	17
β	-1.0E-2	1.0E-2	68
t	0.0	3.0	17

the energy level is within the allowed range, the set of initial conditions is converted to the system of the ephemeris model, and then saved for further use.

A.4. Propagation

For each of the initial conditions that are found through the method describes in Section A.3, a full trajectory is propagated. This is done using the Cowell propagator and Runge-Kutta-Fehlberg 7(8) integrator that are available in TUDAT. The following settings were used for the Sun-Earth system:

Initial Step Size	1.0 sec
Minimum Step Size	500.0 sec
Maximum Step Size	1.0 sec
Relative Error Tolerance	1.0E-20
Absolute Error Tolerance	1.0E-12
Propagation Time	0.7 sidereal years

For the Earth-Moon system, the following settings were used:

Initial Step Size	1.0 sec
Minimum Step Size	0.1 sec
Maximum Step Size	50.0 sec
Relative Error Tolerance	1.0E-20
Absolute Error Tolerance	1.0E-12
Propagation Time	0.3 sidereal years

It should be noticed that in case of stable asymptotic trajectories, backwards propagation is required. For transit and non-transit trajectories, both forward and backward propagation is required, both at half the full propagation time.

The resulting trajectories are saved with 1000 states per trajectory, linearly divided over the original set of states. This means that in those areas where the propagator used a small time-step, there will still be more states saved. The files are all given a name which includes the values of α_1 , α_2 , β , t , and an indicator of the trajectory class.

Bibliography

- Abraham, R., Marsden, J., and Ratiu, T. (1990). *Manifolds, Tensor Analysis and Applications*. Springer-Verlag.
- Alexander, J. et al. (1975). Scientific instrumentation of the radio-astronomy-explorer-2 satellite. *Astronomy and Astrophysics*, 40.
- Barden, B., Howell, K., and Lo, M. (1996). Application of dynamical systems theory to trajectory design for a libration point mission. Technical report, American Institute of Aeronautics and Astronautics.
- Belbruno, E. (2004). *Capture Dynamics and Chaotic Motions in Celestial Mechanics*. Princeton University Press, 1st edition.
- Bentum, M., Verhoeven, C., and Boonstra, A. (2009). OLFAR - orbiting low frequency antennas for radio astronomy. Technical report, Technology Foundation.
- Betts, J. T. and Erb, S. O. (2003). Optimal low thrust trajectories to the Moon. *SIAM Journal of Applied Dynamical Systems*, 2(2).
- Boyce, W. and DiPrima, R. (2010). *Elementary Differential Equations and Boundary Value Problems*. John Wiley and Sons (Asia), 9th edition.
- Bruns, H. (1887). *Über die Integrale des Vielkörperproblems*. B.G. Teubner.
- Burnett, D., Barraclough, B., Bennett, R., Neugebauer, M., Oldham, L., Sasaki, C., Sevilla, D., Smith, N., Stansbery, E., D.Sweetnam, and Wiens, R. (2003). The Genesis discovery mission: Return of Solar matter to Earth. *Space Science Reviews*, 105.
- Conley, C. (1968). Low energy transit orbits in the restricted three-body problem. *SIAM Journal of Applied Mathematics*, 16(4).
- Davis, K., Born, G., and Butcher, E. (2013). Transfer to Earth-Moon L3 Halo orbits. *Elsevier Acta Astronautica*, 88.
- Dekens, E., Engelen, S., and Noomen, R. (2014). A satellite swarm for radio astronomy. *Acta Astronautica*, 102.
- Delft University of Technology (2016). TUDAT documentation. <http://tudat.tudelft.nl>. visited on: 23/11/2016.
- Engelen, S., Verhoeven, C., and Bentum, M. (2010). OLFAR, a radio telescope based on nano-satellites in Moon orbit. *24th Annual AIAA/USU Conference on Small Satellites*.
- Fehlberg, E. (1969). Low-order classical Runge-Kutta formulas with stepsize control and their application to some heat transfer problems. Technical report, NASA.
- Guzman, J. J., Cooley, D. S., Howell, K. C., and Folta, D. C. (1998). Trajectory design strategies that incorporate invariant manifolds and swingby. *AAS/GSFC 13th International Symposium on Space Flight Dynamics*, 2.
- Howell, K., Beckman, M., Patterson, C., and Folta, D. (2006). Representations of invariant manifolds for applications in three-body systems. *The Journal of the Astronautical Sciences*, 52.
- Jester, S. and Falcke, H. (2009). Science with a lunar low-frequency array: From the dark ages of the universe to nearby exoplanets. *New Astronomy Reviews*, 53.

- Koon, W., Lo, M., Marsden, J., and Ross, S. (2001). Low energy transfer to the Moon. *Celestial Mechanics and Dynamical Astronomy*, 81.
- Koon, W. S., Lo, M. W., Marsden, J. E., and Ross, S. D. (1999). The Genesis trajectory and heteroclinic connections. *AAS*, 99(451).
- Koon, W. S., Lo, M. W., Marsden, J. E., and Ross, S. D. (2000a). Constructing a low energy transfer between Jovian moons. Technical report, Caltech.
- Koon, W. S., Lo, M. W., Marsden, J. E., and Ross, S. D. (2000b). Heteroclinic connections between periodic orbits and resonance transitions in celestial mechanics. Technical report, CalTech.
- Langemeijer, K. (2018). Connecting hyperbolic invariant manifolds at variations of the Poincaré section orientation. Master's thesis, Delft University of Technology.
- Lay, D. (1994). *Linear Algebra and Its Applications*. Pearson Education, Inc., 4th edition.
- Lo, M. and Ross, S. (2001). The lunar L1 gateway: Portal to the stars and beyond. *AIAA Space 2001 Conference*.
- Mingotti, G., Topputo, F., and Bernelli-Zazzera, F. (2010). Efficient invariant-manifold, low-thrust planar trajectories to the moon. Technical report, Institut für Industriemathematik, Universität Paderborn.
- Mingotti, G., Topputo, F., and Mernelli-Zazzera, F. (2011). Optimal low-thrust invariant manifold trajectories via attainable sets. *Journal of Guidance, Control and Dynamics*, 34(6).
- Newton, I. (1687). *Philosophiae Naturalis Principia Mathematica*. Benjamin Motte.
- Ozimek, M. and Howell, K. (2010). Low-thrust transfers in the Earth-Moon system, including applications to libration point orbits. *Journal of Guidance, Control and Dynamics*, 33(2).
- Parker, J. S. (2007). Low-energy ballistic lunar transfers. Technical report, University of Colorado.
- Poincaré, H. (1893). *Les méthodes nouvelles de la mécanique céleste*. Gauthier-Villars.
- Riesbroek, R. and Janin, G. (2000). Ways to the moon. *ESA bulletin*, 103.
- Szebehely, V. and Mark, H. (1998). *Adventures in Celestial Mechanics*. John Wiley and Sons, 2nd edition.
- Topputo, F., Vasile, M., and Bernelli-Zazzera, F. (2005). Low energy interplanetary transfers exploiting invariant manifolds of the restricted three-body problem. Technical report, American Institute of Aeronautics and Astronautics.
- Uesugi, K., Matsuo, H., Kawguchi, J., and Hayashi, T. (1991). Japanese first double lunar swingby mission "hiten". *Acta Astronautica*, 25(7).
- van der Ham, L. (2012). Interplanetary trajectory design using dynamical systems theory. Master's thesis, Delft University of Technology.
- Vermeiden, H. (2014). Optimal translunar lagrange point orbits for OLFAR. Master's thesis, Delft University of Technology.
- Wakker, K. (2015). *The Fundamentals of Astrodynamics*. Delft University of Technology.
- Wertz, J., Everett, D., and Puschell, J. (2011). *Space Mission Engineering: The New SMAD*. Microcosm Press, 1st edition.
- Wiggins, S. (2003). *Introduction to Applied Nonlinear Dynamical Systems and Chaos*. Springer.